Additional Information	NOTICE: This is the author’s version of a work that was accepted for publication in Lithos. Changes resulting from the publishing process, such as peer review, editing, corrections, structural formatting, and other quality control mechanisms may not be reflected in this document. Changes may have been made to this work since it was submitted for publication. A definitive version was subsequently published in Lithos, Vol.174, (2013). doi: 10.1016/j.lithos.2012.07.015

Palaeomagnetic, geochronological and geochemical study of Mesoproterozoic Lakhna Dykes in the Bastar Craton, India: implications for the Mesoproterozoic supercontinent

Sergei A. Pisarevsky[a,b,c,*], Tapas Kumar Biswal[d], Xuan-Ce Wang[b], Bert De Waele[e], Richard Ernst[f,g], Ulf Söderlund[h], Jennifer A. Tait[a], Kamleshwar Ratre[d], Yengkhom Kesorjit Singh[d], Mads Cleve[h]

[a] *The Grant Institute, University of Edinburgh, King's Buildings, Edinburgh, UK, EH9 3JW*

[b] *ARC Centre of Excellence for Core to Crust Fluid Systems (CCFS) and The Institute for Geoscience Research (TIGeR), Department of Applied Geology, Curtin University, GPO Box U1987, Perth, WA 6845, Australia. E-mail: Sergei.Pisarevskiy@curtin.edu.au*

[c] *School of Earth and Environment, University of Western Australia, 35 Stirling Highway, Crawley, WA 6009, Australia. E-mail:Sergei.Pisarevsky@uwa.edu.au*

[d] *Department of Earth Sciences, Indian Institute of Technology Bombay, Powai, Mumbai, 400076. E-mail: tkbiswal@iitb.ac.in*

[e] *SRK Consulting, 10 Richardson Street, WA6005 West Perth, Australia*

[f] *Department of Earth Sciences, Carleton University, Ottawa, K1S5B6, Canada*

[g] *Ernst Geosciences,43 Margrave Avenue, Ottawa, K1T3Y2, Canada*

[h] *Department of Geology, Lund University, Sölvegatan 12, SE-223 62 Lund, Sweden*

Abstract

Palaeomagnetic analysis of the Lakhna Dykes (Bastar Craton, India) yields a palaeopole at 36.6°N, 132.8°E, dp=12.4°, dm=15.9°, and the U-Pb zircon age obtained from one of the rhyolitic dykes is 1466.4 ± 2.6 Ma (MSWD=0.21, concordia age based on two analyses with identical Pb/U ages), similar to previously published U-Pb ages. Major and trace element analyses of the Lakhna Dykes show shoshonitic and high-K calc-alkaline affinities consistent with a subduction related characteristics suggesting an active continental margin setting. This is in keeping with the Palaeo- to Mesoproterozoic tectonic environments in the eastern Indian margin. The new 1460 Ma Indian palaeopole was used to test possible palaeopositions of India within the Mesoproterozoic supercontinent Columbia. Of the four palaeomagnetically permissible reconstructions, juxtaposing western India against south-west Baltica is geologically the most reliably constrained and best fitting

[*] *Corresponding author; telephone: +61 8 6488 5076; fax: +61 8 6488 1037; e-mail: Sergei.Pisarevsky@uwa.edu.au*

model. Our preferred reconstruction implies a long Palaeo- to Mesoproterozoic accretionary orogen stretching from south-eastern Laurentia through south-western Baltica to south-eastern India. Breakup of India and Baltica probably occurred in the Late Mesoproterozoic, but additional constraints are needed.

Keywords: *paleomagnetism; dykes; supercontinent; Columbia; Proterozoic; India.*

1. Introduction

An increasing number of publications indicates a growing interest in the Mesoproterozoic palaeogeography and to a hypothetic pre-Rodinian supercontinent variously called Nuna, or Columbia, or Hudsonland (e.g., Hoffman, 1997; Condie, 2000; Meert, 2002; Rogers and Santosh, 2002, 2009; Pesonen et al., 2003; Zhao et al., 2004; Wingate et al., 2009; Pisarevsky and Bylund, 2010; Evans and Mitchell, 2011; Meert, 2012). One of the main reasons for the Columbia hypothesis lies in the widespread evidence for 2.1-1.8 Ga orogens in the majority of Mesoproterozoic continents (e.g., Condie, 2000; Zhao et al., 2004 and references therein) and the suggestion that some or all of these orogens resulted from a supercontinental assembly. Unfortunately, most Columbia reconstructions are highly speculative and sometimes technically incorrect mostly due to a deficit of high quality Late Palaeoproterozoic and Mesoproterozoic palaeomagnetic data. For example, Evans and Pisarevsky (2008) argue that out of 600 published 1600-1200 Ma palaeopoles (Pisarevsky, 2005) for all Precambrian cratons, only eight satisfy all necessary reliability criteria. A few more recently reported palaeomagnetic poles (e.g., Halls et al., 2006; Salminen and Pesonen, 2007; Bispo-Santos et al., 2008, 2012; Lubnina et al., 2010; Pisarevsky and Bylund, 2010) have improved the situation somewhat, but there are still not enough poles to construct an adequate Apparent Polar Wander Path (APWP) for any one craton, let alone the globally disparate cratons. However, the presence of pairs of precisely coeval palaeopoles from the same two cratonic blocks can provide a palaeomagnetic test of the assumption that these two continents drifted together as parts of a larger supercontinent (Buchan, 2007; Evans and Pisarevsky, 2008). Luckily there are a few such pairs between 1800 and 1000 Ma: there are reliable palaeopoles from both Laurentia and Baltica at 1780-1740 Ma, 1480-1460 Ma and

1270-1260 Ma (see Table 2 of Pisarevsky and Bylund, 2010). Additionally there are coeval poles from Siberia and Laurentia at 1480-1460 Ma and even coeval fragments of APWPs for these two continents for ca. 1050-1000 Ma (Pisarevsky et al., 2008; Wingate et al., 2009). These data suggest that these three continents (Laurentia, Baltica and Siberia) could all have been part of a single supercontinent between 1500 and 1270 Ma (Wingate et al., 2009). Published palaeomagnetic data from other continents are not sufficient to establish their relationships with this supercontinent.

Ratre et al. (2010) reported a ca. 1450 Ma U-Pb SHRIMP age for the Mesoproterozoic Lakhna dyke swarm located in the eastern part of the Bastar Craton in India (Fig.1). This age is very close to the 1480-1460 Ma ages of the abovementioned reliable palaeopoles for Laurentia, Baltica and Siberia. Here we report the results of palaeomagnetic and geochemical studies of the Lakhna Dykes and their implications for the relationship of India and the proposed Mesoproterozoic supercontinent Columbia.

2. Geology and sampling

Cratonic India comprises the Dharwar, Bastar, Singhbhum, Aravalli and Bundelkhand cratons (e.g. Meert et al., 2010 and references therein; Fig. 1a). The southern cratons (Dharwar, Bastar and Singhbhum) are separated from the northern cratons (Aravalli and Bundelkhand) by the Central India Tectonic Zone (CITZ) or the Satpura Belt. The eastern part of the CITZ was formed during accretion of the Bastar and the Singhbhum cratons to the northern Bundelkhand Craton (Meert et al., 2010 and references therein). The timing of this amalgamation is contentious. Some workers suggest that the main collision occurred at ca. 1500 Ma (Yedekar et al., 1990; Roy and Prasad, 2003), but significant crustal shortening is also reported at ca. 1100 Ma (Roy and Prasad, 2003; Roy et al., 2006). On the other hand, Stein et al. (2004) suggest that the entire Indian cratonic assemblage stabilised during the interval 2.50–2.45 Ga and that all younger displacements were minor.

The Archaean Bastar Craton is located in the eastern part of India (Fig.1a). It mostly consists of Palaeoarchaean (3.5-3.6 Ga) TTG basement gneisses and granites (Sarkar et al., 1993, Ghosh, 2004; Rajesh et al., 2009) and relatively undeformed and unmetamorphosed Late Archaean - Early Palaeoproterozoic (~2.5 Ga) granites (Sarkar et al., 1993, Stein et al., 2004), with a number of ca.

3500 Ma old large gneissic xenoliths. The Bastar Craton is bounded by the Meso- to Neoproterozoic Eastern Ghats Mobile Belt (EGMB) in the south-east along the Terrane Boundary Shear Zone (TBSZ). The 1650-1550 Ma deformational and metamorphic events in the EGMB (Mezger and Cosca, 1999; Rickers et al., 2001; Dobmeier and Raith, 2003), the occurrences of ophiolitic mélange with ages between 1890 and 1330 Ma (Dharma Rao et al., 2011), and the development of foreland basins (Biswal et al., 2003; Chakraborty et al., 2010) all suggest a long-lived Mesoproterozoic active margin setting along the south-eastern edge of India in the late Palaeoproterozoic and Mesoproterozoic (e.g. Meert et al., 2010) . The EGMB also records pervasive high-grade metamorphism and deformation at 985-950 Ma, similar to that identified in the Rayner Complex of Eastern Antarctica (e.g., Harley, 2003; Collins and Pisarevsky, 2005 and references therein; Korhonen et al., 2011), and on the basis of which an earliest Neoproterozoic collision is postulated between proto-India (including the Napier Complex) and the Archaean Ruker Terrane of the southern Prince Charles Mountains, to form the India-Napier-Ruker-Rayner continent (Harley, 2003).

Proterozoic dykes are wide spread in the Bastar Craton (e.g. Srivastava, 2006; French et al., 2008; Ernst and Srivastava, 2008; Meert et al., 2010, 2011). Many are undated, but there are at least two mafic igneous events at ~2.3 Ga and at ~1.9 Ga. There are also younger dykes, but many of them are still undated (Meert et al., 2010 and references therein). Dykes which are chemically comparable with the Wai Subgroup of the Deccan flood basalts, have been found near Raipur. Two of them have been recently dated at 63.7 ± 2.7 Ma and 66.6 ± 2.2 Ma (whole rock $^{40}Ar/^{39}Ar$, 2σ), which suggests an extension of the Deccan Large Igneous Province far beyond its present exposure (Chalapathi Rao et al., 2011).

Several dykes of mafic to felsic composition (Nanda et al., 1998) collectively called the Lakhna dyke swarm are emplaced into the Bastar basement near the EGMB front in the Lakhna area (Fig.1b). Most trend roughly N-S and the swarm includes rhyolite bodies, trachytes and some dolerite dykes with thicknesses of 10-30 m (Fig.1b). Several smaller dolerite dykes of an EW to NW-SE trend cut the N-S dykes in several places. Two coarse-grained NNW-SSE trending mafic dykes are found in the western part of the studied area (Fig.1b). One coarse-grained deformed gabbro intrusion within the TBSZ is provisionally included into the Lakhna swarm. Ratre et al. (2010) reported zircon U-Pb SHRIMP ages for three Lakhna Dykes Tr (TKB-7), D5 (TKB-6) and G1 (TKB-8): 1442 ± 30 Ma, 1450 ± 22 Ma and 1453 ± 19 Ma respectively (Fig.1b). In 2009 we collected 131 oriented cores for palaeomagnetic analyses from dykes D1-D10, Tr1 and G1 (Fig. 1b). Parts of these cores were used for geochronological and geochemical studies. Dykes are exposed either on the hill slopes, or in small pits. Unfortunately we could not find exposed cross-cuts or well preserved contacts with country rocks, so it was not possible to carry out any baked contact tests. Additionally, 22 samples were collected specifically for geochemical studies. All sampling sites are shown in Fig. 1b.

3. Analytical methods

3.1 Palaeomagnetism

Remanence behaviour was determined by detailed stepwise alternating field (AF) demagnetisation (≤ 20 steps, up to 100 mT), using an AGICO LDA-3A tumbling demagnetiser. Thermal demagnetisation (≤ 20 steps, to 600°C) was also applied using a Magnetic Measurements MMTD1 furnace and the 2G cryogenic magnetometer in the University of Edinburgh. Magnetic mineralogy was investigated from demagnetisation characteristics and, in selected samples, from detailed variation of susceptibility versus temperature (20 to 700°C) obtained using the Bartington meter in conjunction with an automated Bartington furnace. Parts of the collection were studied in the palaeomagnetic laboratories of Oxford University (UK), Utrecht University (Netherlands), University of Western Australia, University of Bergen (Norway) and Luleå University of Technology (Sweden). Magnetisation vectors were identified using Principal Component Analysis (Kirschvink 1980).

3.2 Geochronology

Approximately 100 grams of sample from the Lakhna dyke D5 was processed for U-Pb geochronology at the Department of Geology at Lund University, Sweden, using standard procedures. The ca. <200 μm fraction of crushed material was carefully mixed with water before being loaded in portions (ca. 50 g per portion) on a Wilfley table (for details see Söderlund and Johansson, 2002). U-Pb TIMS analyses were performed at the Laboratory of Isotope Geology (LIG) and at the Natural

History Museum of Stockholm. Further details of mass spectrometry analysis, data reduction and regression are given by Nilsson et al. (this volume).

3.3 Geochemistry

After petrographic examination, the least-altered samples were selected for whole-rock geochemical analyses. The rocks were crushed into small fragments (< 0.5 cm in diameter) before being further cleaned and powdered in a tungsten mill. Quartz was crushed and the mill cleaned using compressed air between each sample to avoid contamination. A small amount of ca. 30 grams was taken from each sample and transferred to plastic containers and sent to the Acme Analytical Laboratories Ltd (Canada) for major and trace element analyses (Acme codes 4A-4B and 1DX). Total abundances of the major oxides and several minor elements were determined on a 0.2 g sample analysed by ICP-emission spectrometry following a Lithium metaborate/tetraborate fusion and dilute nitric digestion, while rare earth and refractory elements were determined by ICP mass spectrometry following a Lithium metaborate / tetraborate fusion and nitric acid digestion of a 0.2 g sample aliquot. In addition, a separate 0.5 g split was digested in Aqua Regia and analysed by ICP Mass Spectrometry for Mo, Cu, Pb, Zn, Ni, As, Cd, Sb and Bi. Based on repeated analyses (n=21) of an in-house reference sample prepared by GEUS (Geological Survey of Denmark and Greenland) the analytical 1 sigma uncertainties are between ±0.4% and ±1.1% for SiO_2, Al_2O_3, Fe_2O_3, MgO, Na_2O, and Ti_2O and between ±2.4 and ±4.8% for K_2O, TiO_2, CaO, MnO and P_2O_5 (Kokfelt, pers. comm., 2012). Results are presented in Table 3.

The geochemical analyses of 22 additional dyke samples representative of this swarm, were carried out using ICP-AES analysis (Jobin-Vyon Horiba, model: Ultima-2), X-ray fluorescence spectrometer (XRF) and ICP-emission spectrometry at the Department of Earth Sciences, Indian Institute of Technology, Bombay. 0.25 grams of powdered sample were fused with 0.75-gram lithium metaborate and 0.25-gram lithium tetraborate in platinum crucibles at a temperature of 1050°C in a muffle furnace. After cooling, the crucible was immersed in 80 ml of 1M HCl contained in a 150 ml glass beaker and then magnetically stirred until the fusion bead had dissolved completely. Then the sample volume was made up to 100 ml in a standard volumetric flask. The same procedure was adopted to make standard solutions and blank sample. The standards used for the analyses include JSy-1 (syenite), JGb-2 (Basalt), JR- 3 (Rhyolite), JG-2 (Rhyolite), JG-1a (Granodiorite) (GSJ Reference standards, 1998). Major, trace and LOI elements were estimated from the above solution by ICP-emission spectrometry. Results are presented in Table 4. The 2σ uncertainties are between 0.004% and 0.3% for SiO_2, Al_2O_3, Fe_2O_3, MgO, CaO, Na_2O and K_2O and between 0.001% and 0.1% for TiO_2, MnO and P_2O_5. Repeated runs give <10% RSD (relative standard deviation) for most trace elements analysed. Results of standard analyses for both laboratories are provided in Appendix C.

4. Transmitted and reflected light microscopy

The studied rhyolites are pink coloured, fine to medium grained rocks consisting of phenocrysts of rounded to amoeboid quartz and euhedral to subhedral alkali feldspar grains (Fig. 2a). The matrix is fine to medium grained and exhibits extensive graphic intergrowth. Magnetite, zircon and green biotite occur as accessory minerals.

The trachytes are fine to medium grained, light greenish to very dark coloured rocks with aphanitic and mesocratic textures (Fig. 2b). Well-developed flow layers, defined by needle-shaped alkali feldspar grains, are present in the rock. Glomeroporphyritic textures are developed due to segregation of multiple feldspar phenocrysts, with flow layers swerving around these aggregates.

The dolerites are dark to greenish coloured medium grained rocks, consisting of plagioclase, augite, opaques (magnetite) and amygdales (Fig. 2c). An intergranular texture is prominently developed, with augite crystals packed within triangular arrays of plagioclase crystals. An intersertal texture is also present where glass occurs inside the arrays.

The alkali gabbros are coarse grained, dark coloured rocks and contain crude mylonitic foliations close to the TBSZ. In the less deformed units, a cumulus texture between plagioclase, orthoclase, hornblende and relict augites has been observed (Fig. 2d). Ophitic and subophitic textures are prominent with randomly oriented euhedral laths of plagioclase embedded fully or partly in larger pyroxene (or hornblende after augite) crystals. In more deformed portions, a low grade metamorphism has transformed the augites to hornblende.

A reflected microsopy study of the dykes reveals that the opaques are dominantly magnetite which are martitised to varying extent. Magnetite grains in dolerite and trachyte cores are coarse, euhedral to subhedral with polygonal crystalline forms. These have been variously altered to martite along cubic, octahedral planes, fractures and grain boundaries (Fig.2e - for dolerite dyke D2, Fig.2f - for trachyte dyke D10). Figure 2g (rhyolite dyke MA1) shows a photomicrograph of a rhyolite sample where the magnetite occurs as very fine grained crystals disseminated throughout the rock. With larger magnification (Fig. 2h) magnetite grains in the rhyolite are found to occur inside quartz and feldspar phenocrysts. The form and mode of occurrence of all these grains indicate the primary nature of magnetite in all studied rock types.

5. Palaeomagnetism

Natural remanent magnetisation (NRM) intensities of samples range from 0.1 to 8.7 A/m for the dolerites, from 1 to 90 mA/m for the trachyte dykes, and from 1 to 200 mA/m for the rhyolite dykes. Magnetic susceptibilities are within $0.5\text{-}30 \times 10^{-3}$, $1.5\text{-}3.9 \times 10^{-4}$ and $4.0\text{-}94.0 \times 10^{-5}$ SI units correspondingly. Twenty samples proved to be very strongly magnetised with chaotic palaeomagnetic directions and are interpreted as having been subjected to lightning strikes. These samples have been excluded from further discussion.

Thermomagnetic curves (low-field magnetic susceptibility versus temperature) for dolerite samples show Hopkinson peaks close to 550°C (Fig. 3), confirming the presence of fine-grained single-domain titanium-poor titanomagnetite.

In the great majority of samples both thermal and AF demagnetisation isolated a single stable bipolar remanence component carried by low-titanium titanomagnetite with unblocking temperatures between 500°C and 580°C. After removal of low-stability, randomly oriented overprints, ten dykes exhibit either a medium to steep downward (D1-D6, D10, Tr1), or upward (D7, D8) direction of remanence (Fig. 4, 5; Table 1). There were no cases of mixed magnetic polarity within one dyke which supports a primary bipolar origin of the remanence. The magnetic remanence of samples from the dolerite dyke

D9 and from the alkali gabbro G1 is chaotic and the results from these dykes were excluded from the interpretations.

In the absence of contact tests we used the following lines of evidence for the primary origin of the stable remanence. First, the study of polished sections and thermomagnetic analysis (Figs. 2 and 3) indicates the presence of small grains of magnetite including single-domain (SD) grains. Single domain magnetite is a highly stable palaeomagnetic recorder, and must be heated close to 580°C to reset its remanence (e.g. Pullaiah et al. 1975; Walton 1980). As the dykes have not been metamorphosed, such reheating is considered unlikely. Second, the presence of polarity reversals between, but not within, intrusions is supportive of a primary remanence. Third, the mean high-temperature remanence direction (both polarities) is different from all younger reliable Indian data (see discussion and McElhinny et al., 2003).

The remanence directions (Table 1) show no correlation with dyke trends nor with rock types, which suggests a relatively short interval of dyke emplacement, which is also supported by the similar ages of the dated dykes. On the other hand, the presence of two polarities indicates that at least one geomagnetic reversal occurred during this interval, which gives an adequate time for averaging out the geomagnetic secular variations. Remanence directions of two dolerite dykes (D4 and D8, the latter – after polarity inversion) fall a bit outside the main group of directions (Table 1), so their exclusion improves the statistics (Table 1, Fig. 5). However, Table 1 and Fig. 5 presents both the mean direction for ten dykes and for eight dykes. The former has been used for the palaeogeographic reconstructions in section 7.

6. Geochronology

A fraction of prismatic (length:width is 1.5-2), slightly pinkish, euhedral zircon grains (and fragments) were separated from the rhyolitic Lakhna dyke D5 (star in Fig. 1b). No overgrowths or xenocrysts (cores) were observed from back-scattered electron imaging confirming the zircons represent a homogenous (single) population with typical magmatic characteristics (Fig. 6). The ca. 50 optically best grains were subjected to physical air abrasion (Krogh, 1982). From these, six grains were selected and combined into two fractions. Both fractions yield results which are >95 concordant and provide a Concordia age of 1466.4 ± 2.6 Ma (MSWD = 0.21), interpreted to date the emplacement of the dyke. The Concordia diagram is shown in Fig. 7 with isotopic data in Table 2. The age is within the precision limits of a previously obtained zircon U-Pb date of 1450 ± 22 Ma from the same dyke (Ratre et al., 2010).

7. Geochemistry

7.1 Major and trace elements

The major and trace element data are presented in Tables 3 and 4. The studied samples fall into the alkalic and sub-alkalic fields (Fig. 8a, on a volatile-free basis). For the mafic samples (SiO_2 <53 wt.%), total alkalis decrease with increasing SiO_2, suggesting source heterogeneity. Two silica over-saturated (SiO_2 = 51-54 wt.%) mafic rocks (MM4 and MM6 from the alkaline gabbro G1, Fig. 1b) have extremely high total alkalis (13-14 wt.%), plotting in the phonolite field (Fig. 8a). Based on the chemical composition of representative fresh samples (Table 3, 4), the studied rocks vary from basanites/basalts/basaltic andesite to trachytes/rhyolites, according to the IUGS nomenclature (Le Bas et al., 1986; Fig. 8a). The samples are characterised by high K_2O at given silica contents and define two trends: an alkali series trend and a sub-alkalic series trend (Fig. 8b). More than half of the samples (19 of 34) fall within the shoshonite field of Peccerillo and Taylor (1976, Fig. 8b).

The studied dykes have a wide range of major element abundances (Table 3). The mafic samples, with SiO_2 = 45 wt.% to 55 wt.%, show a decrease in TiO_2, FeO_{Total}, MgO, and CaO and increase in Al_2O_3 with increasing SiO_2 (see the Harker plots in Appendix A). The andesitic to rhyolitic samples with SiO_2 > 55 wt.% have relatively constant TiO_2 and CaO abundances and display a slow decrease in FeO* and Al_2O_3 with increasing SiO_2. Na_2O variations with SiO_2 clearly indicate two trends within the dykes. Similarly two trends are visible in the magnesium variations.

The alkalic and sub-alkalic mafic dykes display different trace element patterns (Figs. 9-10). The alkalic mafic dykes (Group 1, see also Tables 3 and 4) display enrichment in light rare earth elements (LREE) with $(La/Sm)_N$ (chondrite normalised values) = 2.7 to 4.9 and $(La/Yb)_N$ = 14 to 32, whereas the sub-alkalic mafic dykes (Group 2, see also Tables 3, 4) have LREE-enriched REE patterns with $(La/Sm)_N$= 1.3 to 2.2 and $(La/Yb)_N$ = 1.7 to 3.9 (Fig. 9). Samples MM4, MM8 (alkaline gabbro) from Group 1 are characterised by extremely enriched light rare earth elements (LREE) with $(La/Sm)_N$= 3.9 to 4.9 and $(La/Yb)_N$ = 22 to 32 (Fig. 9). Group 1 displays high enrichment in large ion lithophile elements (LILE) and light rare earth elements (LREE) (Fig. 10). Group 2 exhibits low LILE and LREE except for Th, with relatively flat primitive mantle normalised trace element patterns. The andesitic dykes mainly plot with the alkalic series (Group 1) with uniform REE patterns (Fig. 9) with $(La/Sm)_N$ = 2.7 to 3.0 and $(La/Yb)_N$ = 11 to 14, and flat primitive mantle normalised trace element patterns (Fig. 10). The felsic samples (dacite to rhyolite) exhibit uniform trace element compositions with significant depletion of Eu (Fig. 9).

7.2 Interpretation

7.2.1 Effects of alteration on the geochemical systems

All samples used in this study exhibit low LOI values (0-3.5 wt.%, mostly <2.5 wt.%), suggesting that the effects of alteration on chemical composition are insignificant. Zirconium, an immobile element during low-degree metamorphism and alteration, can be used as an alteration-independent index of geochemical variations. Bivariate plots of Zr against selected trace elements can thus be used to evaluate the element mobilities during alteration (e.g., Polat and Hofmann, 2003; Wang et al., 2008, 2010). The high field strength elements (HFSE, such as Nb, Ta, Ti, Zr, Hf), rare earth elements (REE), Y, and Th are correlated with Zr, indicating that these elements are essentially immobile during alteration. A weaker correlation between abundances of Na and K versus Zr (r = 0.46 for K and 0.56 for Na), imply only a slight effect of deuteric or hydrothermal alteration on these two elements (Appendix B). Rb, alkaline earth (such as Ca, Sr, and Ba), Pb and Mn elements are all scattered, implying varying degrees of mobility.

7.2.2 Crystal fractionation and crustal contamination

The low abundances of MgO, Cr and Ni in the mafic samples in this study indicate significant prior olivine crystal fractionation. The decrease of TiO_2, CaO, FeO_{Total}, and MgO with increasing SiO_2, and the increase of Al_2O_3 with increasing SiO_2 suggest that mafic samples underwent variable crystal fractionation of olivine + clinopyroxene ± Ti-Fe oxides (Appendix A). The kink on trends of TiO_2, Al_2O_3, CaO and FeO_{Total} versus SiO_2 (SiO_2 = 55-60 wt. %) reflects the appearance of plagioclase on the liquidus (Appendix A). This is confirmed by significant depletion of Eu in felsic samples (Fig. 9). The diagrams of Na_2O and K_2O versus SiO_2 (Fig. 8) indicate two distinctive parental magmas: one with high Na_2O (about 8 wt.%) and K_2O (about 3 wt.%) content and another with low Na_2O (about 3 wt.%) and K_2O (< 1 wt.%) content. This is consistent with the two distinctive types of trace element compositions.

The effect of crustal assimilation can be evaluated by comparing the concentration of major elements SiO_2 and MgO, with trace element ratios of Nb/La, Th/La and La/Yb. The lack of correlations between SiO_2 (MgO) and Nb/La, Th/La, and La/Yb (Fig. 11) implies that crustal contamination played an insignificant role in the generation of these dykes.

7.2.3 Magma source characteristics and petrogenesis

The two types of basaltic samples display distinctive trace element and alkaline signatures, implying derivation from different source regions. Basaltic samples of Group 1 are not normal products of melting of mantle peridotite as indicated by their extremely high trace element concentrations. For instance, the typical Group 1 samples MA4, MM4 and MM8 have about 10 times of an average of typical alkaline OIB (Fig. 9). We interpret this distinct geochemical signature to suggest that they derived from a hydrous mantle source, reflecting the contribution of melt released from the subducted slab and/or melts (Polat et al., 2011, 2012).

Basalts of Group 2 display a large range of trace element compositions without significant depletion of Nb, Zr, Hf and Ti, broadly similar to typical alkaline OIB. Compared to Group 1 basalts, they are characterised by relatively low SiO_2 (50-44 wt.%) and high FeO_{Total} (14-12 wt.%) and TiO_2 (1.6-3.6 wt.%) contents. These features suggest that these basaltic samples were likely directly derived from asthenospheric mantle.

Analysed andesitic dykes mainly belong to alkalic series with an OIB-like trace element pattern, similar to mafic samples of Group 2. Thus, the Group 2 basalts may be the parental magma of these andesitic samples. The trachytic to rhyolitic samples exhibit relatively uniform trace element patterns. These felsic dykes are characterised by enrichment of potassium and plot within the fields ranging from high-K calc-alkaline to shoshonitic series. Shoshonitic series generally have restricted spatial and temporal distribution, and the ultimate origin of the magmatism has commonly been related to thermal events in the mantle, usually related to collision events, such as slab break-off (e.g., Aldanmaz et al., 2000; Kay and Mahlburg Kay, 1993; Morrison, 1980; Pe-Piper et al., 2009). The generation of shoshonites is generally thought to be related to incorporation of subducted sediments in the active continental margin, but also can be produced within an intraplate tectonic setting by partial melting of sub-continental lithospheric mantle (SCLM) which has been metasomatically enriched in an earlier subduction event (Scarrow et al., 2008).

8. Discussion

8.1 Tectonic setting of the Lakhna Dyke Swarm

Based on major element geochemistry only, Ratre et al. (2010) proposed that the Lakhna dyke swarm may have been generated within an extensional tectonic setting, as earlier suggested by Nanda et al. (1998). However, as shown in Fig. 1b, the dyke swarm can be divided into sub-groups according to their orientation. The two sub-groups are nearly perpendicular, but have the same ages, which seems inconsistent with a typical rift setting.

The new geochemical data (major and trace element) clearly indicate shoshonitic and high-K calc-alkaline affinities, consistent with a subduction related setting, with the former representing late stage arc-magma (Scarrow et al., 2008). The coexistence of high-K calc-alkaline with shoshonitic series is favoured here to reflect an active continental margin setting in accord with other studies (e.g., Dharma Rao et al., 2011, 2012; Santosh, 2012).

8.2 Palaeomagneticaly permissive positions of India in Columbia.

The available palaeomagnetic data permit a fixed configuration between Laurentia, Baltica and Siberia from ~1500 Ma to ~1270 Ma (Salminen and Pesonen, 2007; Wingate et al., 2009; Pisarevsky and Bylund, 2010) suggesting that they formed a part of Columbia. Our new 1465 ± 3 Ma Indian palaeopole is coeval to the highly reliable poles from these continents (Table 5; Fig. 12), providing an opportunity to test possible positions of India in Columbia. Of course, it must be borne in mind that: (i) India could be unconnected to Columbia; (ii) India could be juxtaposed not to Laurentia, Baltica or Siberia, but to some other part of Columbia, whose position is not yet constrained. With these limitations our new palaeopole allows four reconstructions with India juxtaposed against Laurentia, Baltica, or Siberia (Fig. 12a-d) at 1460 Ma.

Using other precisely dated Mesoproterozoic Indian palaeopoles (Table 5, entries 29-32) and coeval poles from Laurentia, Baltica and Siberia, we shall test the viability of these reconstructions at ca. 1190, 1120 and 1080 Ma. Euler rotation parameters for Laurentia, Baltica and Siberia are listed in Table 6 and the rotation parameters for India are given in figure captions.

The 1192 ± 10 Ma Harohalli pole (Table 5, entry 29) is coeval to two Laurentian poles from the 1184 ± 5 Ma intrusions in Greenland (Table 5, entries 8 and 9). Figure 13a demonstrates that the 1460 Ma reconstruction of India juxtaposed to SE Laurentia (Fig. 12a) could not have persisted until 1190 Ma. The corresponding Euler rotation parameters applied to the Indian pole move it to low latitudes ~60° away from the geographic pole approximated by Laurentian palaeopoles, implying India-Laurentia separation before ca. 1190 Ma. The ca. 1080 Ma Indian palaeopoles are also discordant with coeval Laurentian poles in the tested reconstruction (Table 5, Fig. 13a).

Geological data are also not supportive to the India – SE Laurentia fit. The SE edge of Laurentia has been a long-lived 1.8 – 1.0 Ga convergent orogen (e.g., Karlstrom et al., 2001). The eastern edge of India should also be considered as long-lived active margin during roughly the same time interval (see Section 8.1). Figure 12a shows that the India – SE Laurentia reconstruction requires juxtaposition of two active continental margins with opposite directions of tectonic transport thus discounting this reconstruction as a viable option.

As shown in Fig.12b and 13b, palaeomagnetic data permit positioning of India against the western margin of Laurentia (present-day co-ordinates) from 1460 Ma until 1190 Ma, given that the circles of 95% confidence for the Laurentian and Indian poles overlap. However, if such a connection existed, palaeomagnetic data dictate that it must have been broken before 1080 Ma (Fig. 13b).

The western margin of Laurentia contains a rift – passive margin succession initiated at c. 750 Ma (e.g., Moores, 1991; Ross et al., 1995; Dehler et al., 2010). It remains a matter of debate as to which continent separated from this Laurentian margin, possible candidates including: Australia (e.g., Moores, 1991; Dalziel, 1991; Hoffman, 1991; Brookfield, 1993; Karlstrom et al., 1999; Burrett and Berry, 2000; Wingate et al., 2002), South China (Li et al., 1995), Siberia (Sears and Price, 2000), West Africa, or Rio de La Plata (Evans, 2009). Late Mesoproterozoic palaeomagnetic data rule out an Australia-Laurentia connection at ~1.2 Ga (Pisarevsky et al., 2003). A Siberia-W. Laurentia fit also failed palaeomagnetic tests and has problems with geological mismatches (Pisarevsky and Natapov, 2003; Pisarevsky et al., 2008). A lack of reliable Mesoproterozoic palaeomagnetic data prevents similar tests for South China, West Africa and Rio de La Plata.

Major geological features (Fig. 12b) permit connections between the Archaean Dharwar Craton and the displaced fragment of the Slave Craton, and also between Indian Aravalli and Bundelkhand cratons, and Hearne, Wyoming and Medicine Hat blocks of Laurentia. The earliest deformations in CITZ (2100-1900 Ma; Mohanty, 2010) are similar in age to those in the Taltson Belt of Laurentia (Hoffman, 1989). Both orogens have the same trend in this reconstruction. This reconstruction also juxtaposes the Lakhna magmatism with the widespread coeval magmatism in adjacent western Laurentia (e.g., Anderson and Davis, 1995; Ernst and Buchan, 2001; Ernst et al., 2008; Harlan et al., 2008). However, in our preferred interpretation of the geochemistry the Lakhna Dykes are associated with subduction processes, which would contradict this comparison. The timing of sedimentation in the Mesoproterozoic Belt Basin (Fig. 12b) in Laurentia (e.g., Luepke and Lyons, 2001) is overlapping with that in Vindhyan basins of India (Malone et al., 2008; Meert et al., 2010). According to palaeomagnetic data (Figs. 12b, 13b) the separation of India from Laurentia should occur between 1190 and 1080 Ma. However, there is strong evidence that continental breakup along the western

Laurentian margin occurred not earlier than ca. 750 Ma (e.g., Moores, 1991; Ross et al., 1995; Dehler et al., 2010).

There are no reliable Siberian palaeopoles between ca. 1460-1050 Ma (Table 5). However, there is good evidence that Laurentia and Siberia were in a fixed position with respect to each other between ca. 1470 -1000 Ma (Wingate et al., 2009). Consequently the 1460-1050 Ma Laurentian poles can be used for palaeomagnetic testing of the western India – SW Siberia reconstruction (Fig. 12c) at 1190 Ma and 1080 Ma (Fig. 13c). As in the previous case, the proposed India-Siberia reconstruction is palaeomagnetically permissive at 1190 Ma, but not later. Geological data do not support juxtaposition of India and SW Siberia in the Mesoproterozoic (Fig. 12c). First, even though the Archaean Dharwar Craton and the Archaean Tungus Terrane are close in this reconstruction, they are separated by the ca. 1.9 Ga Angara orogenic belt (Rosen et al., 1994; Condie and Rosen, 1994), which contradicts the idea of their common origin. Second, Gladkochub et al. (2006a, b) demonstrated that the continental breakup and sedimentation on the SW Siberian passive margin did not commence until after ca. 750 Ma. We conclude that the proposed India-Siberia reconstruction is not viable.

Fig. 12d shows the fourth reconstruction with the Dharwar Craton of India juxtaposed to Sarmatia (Baltica). The VGP from the 1122 ± 7 Ma Salla dyke of Baltica (Table 5) is, within the error limits, coeval to the 1113 ± 7 Ma Mahoba palaeopole from India (Pradhan et al., 2012). Circles of confidence of these poles overlap (Fig. 13d), so it is possible that at that time India and Baltica were still together. Palaeopoles for Baltica and India at ca. 1080 Ma demonstrate that the two continents must have separated by this time. Hence the Baltica-India reconstruction shown in Fig. 12d could be true from 1460 Ma until 1120 Ma. In the tested reconstruction the Archaean Dharwar and Sarmatia cratons are located next to each other (Fig. 12d) suggesting that they formed part of a single proto-craton. Sarmatia consists of several terranes which welded together in the latest Archaean – earliest Palaeoproterozoic (Bogdanova et al., 1996). The Dharwar Craton has a somewhat similar history whereby the eastern and western parts were welded together at ca 2515 Ma (Meert et al., 2010). Late Archaean and Palaeoproterozoic banded iron formations (BIFs) are widespread in Sarmatia and Dharwar (Fig. 12d). Sarmatia is bounded by the 2.10-2.02 Ga Lipetsk-Losev/East Voronezh Belt

(Fig. 12d; Schipansky et al., 2007; Bogdanova et al., 2008). Deformation and UHT metamorphism of similar age (2040 ± 17 Ma) has been reported from CITZ (Mohanty, 2010, 2012). Trends and positions of these two orogens also suggest their possible relationship (Fig. 12d). Many Mesoproterozoic (ca. 1.4-1.0 Ga) kimberlites and lamproites are reported both from Dharwar and Sarmatia (e.g., Chalapathi Rao et al., 2004; Kumar et al., 2007; Bogatikov et al., 2007), however, many of these are not precisely dated, precluding any direct correlations.

An India-Baltica reconstruction (Fig. 12d) aligns the eastern margin of India with the southern segment of the SW margin of Baltica. The Proterozoic tectonic history of Baltica is characterised by the prolonged accretion from the present west (Fig. 12b; Gorbatschev and Bogdanova, 1993; Bogdanova et al., 2001; Åhäll and Connelly, 2008; Bingen et al, 2008; Bogdanova et al., 2008). The 1.85-1.33 Ga ophiolitic melange in the EGMB of India (Fig. 12d; Dharma Rao et al., 2011) suggest a long-lived active margin environment along the eastern Indian margin. This is supported by the development of foreland basins (Biswal et al., 2003; Chakraborty et al., 2010) and by geochemical data (see above). It was previously suggested that the SW Palaeo- to Mesoproterozoic active margin of Baltica is a continuation of the accretionary margin of Laurentia (e.g., Karlstrom et al., 2001; Pisarevsky and Bylund, 2010). If our hypothesis is correct, this implies a giant nearly linear long-lived Palaeo- to Mesoproterozoic 'Laurentia-Baltica-India' accretionary orogen comparable in scale with the present eastern Pacific active margin.

Palaeomagnetic data suggest that India broke up from Baltica between ca. 1120 and 1080 Ma. However, there is no evidence of Mesoproterozoic rifting in the western Dharwar Craton. Such evidence could be concealed in the recently rifted Seychelles Block and/or Antongil Terrane of Madagascar. However, these blocks were strongly tectonically overprinted in Neoproterozoic and Cambrian times (Tucker et al., 2001; Schofield et al., 2010). Similarly, the SW margin of Sarmatia is mostly covered and probably overprinted by the Cadomian orogeny. Bogdanova et al. (1996) suggested that the 1.3-1.1 Ga Volyn-Orsha Aulacogen (Fig. 12d) could represent the failed-arm of a triple junction, which implies that the successful rifting could occur along the Teisseyre-Tornquist line, which may also represent the rifting between Baltica and India. Poprawa and Pacześna (2002) suggested that this rifting could have occurred during the Mesoproterozoic. The 1.3-1.1 Ga mafic sills in the western part of the Volyn-Orsha Aulocogen (Bogdanova et al., 2008) indirectly provide some constraints on the timing of rifting between Baltica and India.

Altogether among other discussed possibilities this reconstruction with India juxtaposed to Baltica is considered to be the most robust model.

9. Conclusions

1. A new U-Pb age of 1465 ± 3 Ma from the rhyolitic D5 Lakhna Dyke in the Bastar Craton of India is similar to previously published U-Pb zircon dates of this and two other dykes of the Lakhna Dyke Swarm.

2. Geochemical data from the Lakhna Dykes indicate shoshonitic and high-K calc-alkaline affinities suggesting that they are related to subduction in an active continental margin setting.

3. A palaeomagnetic study of the Lakhna dykes has provided a new robust 1460 Ma palaeopole for India, which is coeval to reliable palaeopoles from Laurentia, Baltica and Siberia.

4. Indian geology and Precambrian geological data from Laurentia, Baltica and Siberia suggest that, among four palaeomagnetically permissive positions of India, the reconstruction of western India attached to south-west Baltica (Sarmatia) is geologically and palaeomagnetically the most permissible model. The reconstruction implies a long-lived nearly linear Palaeo- to Mesoproterozoic mega-accretionary orogen along south-eastern Laurentia, south-western Baltica and eastern India. This orogen was comparable in terms of scale with the present Cordillieran-Andean orogen in America.

Acknowledgements

Palaeogeographic reconstructions are made with free GPLATES software (http://www.gplates.org/). This is contribution xx from the ARC Centre of Excellence for Core to Crust Fluid Systems, and TIGeR publication #xx and also publication #19 of the LIPs-Supercontinent Reconstruction Project (http://www.supercontinent.org). SP and JT gratefully acknowledge funding from the Marie Curie FP6 Excellence Grant scheme.

References

Aldanmaz, E., Pearce, J.A., Thirlwall, M.F., Mitchell, J.G., 2000. Petrogenetic evolution of late Cenozoic, post-collision volcanism in western Anatolia, Turkey. Journal of Volcanology and Geothermal Research, 102(1-2), 67-95.

Anderson, H.E., Davis, D.W. 1995. U-Pb geochronology of the Moyie sills, Purcell Supergroup, southeastern British Columbia: Implications for the Mesoproterozoic geological history of the Purcell (Belt) basin. Canadian Journal of Earth Sciences 32, 1180-1193.

Åhäll, K-I., Connelly, J.N., 2008. Long-term convergence along SW Fennoscandia: 330 m.y. of Proterozoic crustal growth. Precambrian Research 163, 402-421.

Bingen, B., Andersson, J., Söderlund, U., Möller, C., 2008. The Mesoproterozoic in the Nordic countries. Episodes 31(1), 29-34.

Bispo-Santos, F., D'Agrella-Filho, M.S., Trindade, R.I.F., Elming, S.-Å., Joinikian, L., Vasconcelos, P.M., Perillo, B.M., Pacca, I.I.G., da Silva, J.A., Barros, M.A.S., 2012. Tectonic implications of the 1419 Ma Nova Guarita mafic intrusive paleomagnetic pole (Amazon Craton) on the longevity of Nuna. Precambrian Research 196-197, 1-22.

Bispo-Santos, F., D'Agrella-Filho, M.S., Pacca, I.I.G., Janikian, L., Trindade, R.I.F., Elming, S.-Å., Silva, J.A., Barros, M.A.S., Pinho, F.E.C., 2008. Columbia revisited: Paleomagnetic results from the 1790 Ma colider volcanics (SW Amazonian Craton, Brazil). Precambrian Research 164, 40-49.

Biswal, T.K., Sinha, S., Mandal, A., Ahuja, H., Das, M.K., 2003. Deformation pattern of Bastar craton adjoining Eastern Ghat mobile belt, NW Orissa. Gondwana Geological Magazine, Special Publication 7, 101–108.

Bogatikov, O.A., Kononova, V.A., Nosova, A.A., Kondrashov, I.A., 2007. Kimberlites and lamproites of the east European Platform: petrology and geochemistry. Petrology 15(4), 315-334.

Bogdanova, S.V., Pashkevich, I.K., Gorbatschev, R., Orlyuk, M., 1996. Riphean rifting and major Paleoproterozoic boundaries in the East European Craton: geology and geophysics. Tectonophysics 268, 1–22.

Bogdanova, S. V., Page, L. M., Skridlaite, G., Taran, L. N., 2001. Proterozoic tectonothermal history in the western part of the East European Craton: 40Ar/39Ar geochronological constraints: Tectonophysics 339, 39–66, doi: 10.1016/S0040-1951(01)00033-6.

Bogdanova, S.V., Bingen, B., Gorbatschev, R., Kheraskova, T.N., Kozlov, V.I., Puchkov, V.N., Volozh, Yu.A., 2008. The Eastern European Craton (Baltica) before and during the assembly of Rodinia. Precambrian Research 160, 23–45.

Brookfield, M.E., 1993. Neoproterozoic Laurentia-Australia fit. Geology 21, 683-686.

Buchan, K.L., 2007. Pole, key paleomagmetic. In: Gibbins, D., Herrero-Bervera, E. (eds), Encyclopedia of Geomagnetism and Paleomagnetism. Springer, Dordrecht, Netherlands, pp. 839-840.

Buchan, K. L., Halls, H. C., 1990. Paleomagnetism of Proterozoic mafic dyke swarms of the Canadian Shield. In: Parker, A. J., Rickwood, P. C., Tucker, D. H. (eds), Mafic Dykes and Emplacement Mechanism. Rotterdam, A. A. Balkema, pp. 209–230.

Buchan, K., Ernst, R., Hamilton, M., Mertanen, S., Pesonen, L.J., Elming, S.-Å., 2001. Rodinia: the evidence from integrated paleomagnetism and U–Pb geochronology. Precambrian Research 110, 9 – 32.

Burrett, C., Berry, R., 2000. Proterozoic Australia-Western United States (AUSWUS) fit between Laurentia and Australia. Geology 28, 103-106.

Bylund, G., 1985, Palaeomagnetism of middle Proterozoic basic intrusives in central Sweden and the Fennoscandian apparent polar wander path: Precambrian Research 28, 283–310, doi: 10.1016/0301-9268(85)90035-X.

Chakraborty, P.P., Dey, S., Mohanty, S.P., 2010. Proterozoic platform sequences in Peninsular India: Implications towards basin evolution and supercontinent assembly. Journal of Asian Earth Sci ences 39, 589-607.

Chalapathi Rao, N.V., Gibson, S.A., Pyle, D.M., Dickin, A.P., 2004. Petrogenesis of Proterozoic Lamproites and Kimberlites from the Cuddapah Basin and Dharwar Craton, Southern India. JOurnal of Petrology 54, 907-948.

Chalapathi Rao, N.V., Burgess, R., Lehmann, B., Mainkar, D., Pande, S.K., Hari, K.R., Bodhankar N., 2011. $^{40}Ar/^{39}Ar$ ages of mafic dykes from the Mesoproterozoic Chhattisgarh basin, Bastar craton, Central India: Implication for the origin and spatial extent of the Deccan Large Igneous Province. Lithos 125, 994–1005.

Collins, A.S., Pisarevsky, S.A., 2005. Amalgamating Eastern Gondwana: the evolution of the Circum-Indian orogens. Earth-Science Reviews 71, 229-270. DOI:10.1016/j.earscirev.2005.02.004.

Commission for the Geological Map of the World, 2000. Geological Map of the World at 1:25,000,000. CGMW and UNESCO.

Condie, K.C., 2000. Episodic continental growth models: afterthoughts and extensions. Tectonophysics 322, 153–162.

Condie, K.C., Rosen, O.M., 1994. Laurentia–Siberia connection revisited. Geology 22, 168–170.

Dalziel, I.W.D., 1991. Pacific margins of Laurentia and East Antarctica–Australia as a conjugate rift pair: evidence and implications for an Eocambrian supercontinent. Geology 19, 598–601.

Davis, D., Green,J., 1997. Geochronology of the North American Midcontinent rift in western Lake Superior and implications for its geodynamic evolution. Canadian Journal of Earth Sciences 34,476–488.

Davis, D. W., Paces, J. B., 1990. Time resolution of geologic events on the Keweenaw Peninsula and applications for development of the Midcontinent Rift system. Earth and Planetary Science Letters 97, 54-64.

Dehler, C.M., Fanning, C.M., Link, P.K., Kingsbury, E.M., Rybczynski, D., 2010. Maximum depositional age and provenance of the Uinta Mountain Group and Big Cottonwood Formation, northern Utah: Paleogeography of rifting western Laurentia. Geological Society of America Bulletin 122, 1686-1699.

Dharma Rao, C.V., Santosh, M., Wu, Y-B., 2011. Mesoproterozoic ophiolitic mélange from the SE periphery of the Indian plate: U-Pb zircon ages and tectonic implications. Gondwana Research 19, 384-401.

Dharma Rao, C.V., Santosh, M., Dong, Y., 2012. U–Pb zircon chronology of the Pangidi–Kondapalle layered intrusion, Eastern Ghats belt, India: Constraints on Mesoproterozoic arc magmatism in a convergent margin setting. Journal of Asian Earth Sciences 49, 362–375.

Diehl, J.F., Haig, T.D., 1994. A paleomagnetic study of the lava flows within the Copper Harbor Conglomerate, Michigan: new results and implications. Canadian Journal of Earth Sciences 31, 369-380.

Dobmeier, C.J., Raith, M.M., 2003. Crustal architecture and evolution of the Eastern Ghats Belt and adjacent regions of India. In: Yoshida, M., Windley, B.F., Dasgupta, S. (Eds.), Proterozoic East Gondwana: Supercontinent Assembly and Breakup. Special Publication Geological Society of London, vol. 206, pp. 145– 168.

Emslie, R. F., Irving, E., Park, J. K., 1976. Further paleomagnetic results from the Michikamau intrusion, Labrador. Canadian Journal of Earth Sciences 13, 1052–1057.

Ernst, R.E., Buchan, K.L., 2001. Large mafic magmatic events through time and links to mantle plume heads, in Ernst, R.E., and Buchan, K.L., (eds.), Mantle Plumes: Their Identification Through Time: Geological Society of America Special Paper 352, p. 483–575.

Ernst, R.E., Srivastava, R.K., 2008. India's place in the Proterozoic world: constraints from the large igneous provinces (LIP) record. In: Srivastava, R.K., Sivaji, Ch., and Chalapathi Rao N.V. (eds.) Indian Dykes: Geochemistry, Geophysics, and Geochronology, Narosa Publishing House Pvt. Ltd, New Delhi, India, pp. 41-56.

Evans, D.A.D., 2009. The palaeomagnetically viable, long-lived and all-inclusive Rodinia supercontinent reconstruction. In: Murphy, J.B., Keppie, J.D., Hynes, A. (eds.), Ancient Orogens and Modern Analogues. Geological Society of London Special Publication, vol. 327, pp.371-404.

Evans, D.A.D., Mitchell, R.N., 2011. Assembly and breakup of the core of Paleoproterozoic–Mesoproterozoic supercontinent Nuna. Geology 39, 443-446.

Evans, D.A.D., Pisarevsky, S.A., 2008. Plate tectonics on the early Earth?-weighing the paleomagnetic evidence. In: Condie, K. , Pease, V. (eds). When Did Plate Tectonics Begin? Geological Society of America Special Paper 440, 249-263.

Fisher, R.A., 1953. Dispersion on a sphere, Proc. R. Soc. Lond. A, 217, 295–305.

French, J. E., Heaman, L. M., Chacko, T., Srivastava, R. K., 2008. 1891-1883 Ma Southern Bastar-Cuddapah mafic igneous events, India: a newly recognised large igneous province. Precambrian Research 160, 308-322.

Gallet, Y., Pavlov, V.E., Semikhatov, M.A., Petrov, P.Yu., 2000. Late Mesoproterozoic magnetostratigraphic results from Siberia: paleogeographic implications and magnetic field behaviour. Journal of Geophysical Research 105, 16481–16499.

Geological survey of Japan, Geochemical Reference samples DataBase,1998. (http://www.aist.go.jp/RIODB/geostand/welcome.html)

Ghosh, J. G., 2004. 3.56 Ga tonalite in the central part of the Bastar craton, India: oldest Indian date. Journal of Asian Earth Sciences 23, 359–64.

Gladkochub, D., Pisarevsky, S.A., Donskaya, T., Natapov, L.M., Mazukabzov, A., Stanevich, A.M., Slkyarov, E., 2006a. Siberian Craton and its evolution in terms of Rodinia hypothesis. Episodes 29 (3), 169–174.

Gladkochub, D.P., Wingate, M.T.D., Pisarevsky, S.A., Donskaya, T.V., Mazukabzov, A.M., Ponomarchuk, V.A., Stanevich, A.M., 2006b. Mafic intrusions in southwestern Siberia and implications for a Neoproterozoic connection with Laurentia. Precambrian Research 147, 260–278.

Gorbatschev, R., Bogdanova, S., 1993. Frontiers in the Baltic Shield. Precambrian Research 64, 3–21, doi: 10.1016/0301-9268(93)90066-B.

Gregory, L.C., Meert, J.G., Pradhan, V., Pandit, M.K., Tamrat, E., Malone, S.J., 2006. A paleomagnetic and geochronological study of the Majhgawan Kimberlite, India: implications for the age of the Vindhyan SuperGroup. Precambrian Research 149, 65–75.

Halls, H.C., 1974. A paleomagnetic reversal in the Osler Volcanic Group, northern Lake Superior. Canadian Journal of Earth Sciences 11, 1200-1207.

Halls, H.C., Kumar, A., Srinivasan, R., Hamilton, M.A., 2006. A Mesoproterozoic paleomagnetic pole from the Yangzhuang Formation, North China and its tectonics implications. Precambrian Research 151, 1-13.

Harley, S.L., 2003. Archaean–Cambrian crustal development of East Antarctica: metamorphic characteristics and tectonic implications. In: Yoshida, M., Windley, B.F., Dasgupta, S. (Eds.), Proterozoic East Gondwana: Supercontinent Assembly and Breakup. Special Publication Geological Society of London, vol. 203, pp. 203– 230.

Harlan, S.S., Geissman, J.W., Snee, L.W., 2008. Paleomagnetism of Proterozoic mafic dikes from the Tobacco Root Mountains, southwest Montana. Precambrian Research 163, 239-264.

Henry, S. G., Mauk, E J., Van der Voo, R., 1977. Paleomagnetism of the upper Keweenawan sediments: the Nonesuch Shale and Freda Sandstone. Canadian Journal of Earth Sciences14, 1128-1138.

Hnat, J.S., Van der Pluijm, B.A., Van der Voo, R. 2006. Primary curvature in the Mid-Continent Rift: Paleomagnetism of the Portage Lake Volcanics (northern Michigan, USA). Tectonophysics 425, 71–82.

Hoffman, P.F., 1991. Did the breakout of Laurentia turn Gondwana inside out? Science 252, 1409-1412.

Hoffman, P.F., 1996. Tectonic genealogy of North America. In: van der Pliujm, B.A., Marshak, S. (Eds.), Earth structure: An introduction to structural geology and tectonics. W.W. Norton & Company, New York, 607–614.

Hoffman, P.F., 1989. Precambrian geology and tectonic history of North America. In: Bally, A.W., Palmer, A.R. (eds.), The Geology of North America – an overview. Boulder, Colorado, Geological Society of America, The Geology of North America, A, 447-512.

Irving, E., Baker, J., Hamilton, M., and Wynne, P. J., 2004. Early Proterozoic geomagnetic field in western Laurentia: implications for paleolatitudes, local rotations and stratigraphy. Precambrian Research 129, 251–270, doi: 10.1016/j.precamres.2003.10.002.

Karlstrom, K.E., Harlan, S.S., Williams, M.L., McLelland, J., Geissman, J.W, Åhäll, K.-I., 1999. Refining Rodinia: geologic evidence for the Australia-Western U.S. connection in the Proterozoic. GSA Today 9(10), 1-7.

Karlstrom, K.E., Åhäll, K.I., Harlan, S.S.,Williams, M.L., McLelland, J., Geissman, J.W., 2001. Long-lived (1.8–1.0 Ga) convergent orogen in southern Laurentia, its extensions to Australia and Baltica, and implications for refining Rodinia. Precambrian Research 111, 5–30.

Kay, R.W., Mahlburg Kay, S., 1993. Delamination and delamination magmatism. Tectonophysics 219(1-3), 177-189.

Kean, W.F., Williams., I., Chan,L. , Feeney, J., 1997. Magnetism of the Keweenawan age Chengwatana lava flows, northwest Wisconsin. Geophysical Research Letters 24, 1523-1526.

Khan, R.M.K., Naqvi, S.M., 1996. Geology, geochemistry and genesis of BIF of Kushtagi schist belt, Archaean Dharwar Craton, India. Mineralium Deposita 31, 123-133.

Kirschvink, J.L., 1980. The least squares line and plane and the analysis of palaeomagnetic data, Geophysical Journal of the Royal Astronomic Society 62, 699–718.

Korhonen, F.J., Saw, A.K., Clark, C., Brown, M., Bhattacharya, S., 2011. New constraints on UHT metamorphism in the Eastern Ghats Province through the application of phase equilibria modelling and in situ geochronology. Gondwana Research 20, 764–781.

Krogh, T.G., 1982. Improved accuracy of U-Pb zircon ages by the creation of more concordant systems using an air abrasion technique. Geochimica et Cosmochimica Acta 46, 637-649.

Kumar, A., Heaman, L.M., Manikyamba, C., 2007. Mesoproterozoic kimberlites in south India: a possible link to ~1.1 Ga global magmatism. Precambrian Research 154, 192-204.

Le Bas, M.J., Le Maitre, R.W., Streckeisen, A., Zanettin, B., 1986. A Chemical Classification of Volcanic Rocks Based on the Total Alkali-Silica Diagram. Journal of Petrology 27(3), 745-750.

LeCheminant, A. N., Heaman, L. M., 1989. Mackenzie igneous events, Canada: Middle Proterozoic hotspot magmatism associated with ocean opening. Earth and Planetary Science Letters 96, 38–48, doi: 10.1016/0012-821X(89)90122-2.

Li, Z.X., Zhang, L., Powell, C.M., 1995. South China in Rodinia: part of the missing link between Australia–East Antarctica and Laurentia? Geology 23, 407–410.

Lubnina, N., 2009. The East-European Craton from NeoArchean to Palaeozoic according to the palaeomagnetic data. Unpublished Dr. Sci. Thesis. Moscow State University, Moscow, 44 pp.

Lubnina, N.V., Mertanen, S., Soderlund, U., Bogdanova, S.V., Vasilieva, T.I., Frank-Kamenetsky, D., 2010. A new key pole for the East European Craton at 1452 Ma: Palaeomagnetic and geochronological constraints from mafic rocks in the Lake Ladoga region. Precambrian Research 183, 442-462.

Luepke, J.J., Lyons, T.W., 2001. Pre-Rodinian (Mesoproterozoic) supercontinental rifting along the western margin of Laurentia: geochemical evidence from the Belt-Purcell Supergroup. Precambrian Research 111, 79-90.

Malone, S.J., Meert, J.G., Banerjee, D.M., Pandit, M.K., Tamrat, E., Kamenov, G.D., Pradhan, V.R., Sohl, L.E., 2008. Paleomagnetism and detrital zircon geochronology of the Upper Vindhyan sequence, Son Valley and Rajasthan, India: a ca. 1000 Ma closure age for the Purana basins? Precambrian Research164, 137–159.

McCabe, C., Van der Voo, R., 1983. Paleomagnetic results from the upper Keweenawan Chequamegon Sandstone: implications for red bed diagenesis and Late Precambrian apparent polar wander of North America. Canadian Journal of Earth Sciences, 20, 105-112.

McElhinny, M. W., Powell, C. M., Pisarevsky, S. A., 2003. Paleozoic terranes of eastern Australia and the drift history of Gondwana, Tectonophysics 362, 41–65.

Meert, J.G., 2002. Paleomagnetic evidence for a Paleo-Mesoproterozoic supercontinent Columbia: Gondwana Research 5, 207–215.

Meert, J.G., 2012. What's in a name? The Columbia (Paleopangaea/Nuna) supercontinent. Gondwana Research 21, 987-993.

Meert, J.G., Stuckey, W., 2002. Revisiting the paleomagnetism of the 1.476 Ga St. Francois Mountains igneous province, Missouri. Tectonics 21, 1007, doi:10.1029/2000TC001265.

Meert, J.G., Torsvik, T.H., 2003. The making and unmaking of a supercontinent: Rodinia revisited. Tectonophysics 375, 261–288.

Meert, J.G., Pandit, M.K., Pradhan, V.R., Banks, J., Sirianni, R., Stroud, M., Newstead, B., Gifford, J., 2010. Precambrian crustal evolution of Peninsular India: 3.0 billion year odyssey. Journal of Asian Earth Sciences 39, 483-515.

Meert, J.G., Pandit, M.K., Pradhan, V.R., Kamenov, G., 2011. Preliminary report on the paleomagnetism of 1.8 Ga dykes from the Bastar and Dharwar cratons, Peninsular India. Gondwana Research 20, 335-343.

Mertanen, S., Pesonen, L.J., Huhma, H., 1996. Palaeomagnetism and Sm-Nd ages of the Neoproterozoic diabase dykes in Laanila and Kautokeino, northern Fennoscandia. In: Brewer, T.S. (ed), Precambrian Crustal Evolution in the North Atlantic region, Geological Society of London Special Publication, vol. 112, pp. 331-358.

Mezger, K., Cosca, M., 1999. The thermal history of the Eastern Ghats Belt (India), as revealed by U–Pb and $^{40}Ar/^{39}Ar$ dating of metamorphic and magmatic minerals: implications for the SWEAT hypothesis. Precambrian Research 94, 251– 271.

Mohanty, S., 2010. Tectonic evolution of the Satpura Mountain Belt: a critical evaluation and implication on supercontinent assembly. Journal of Asian Earth Sciences 39, 516-526.

Mohatny, S., 2012. Spatio-temporal evolution of the Satpura Mountain Belt of India: A comparison with the Capricorn Orogen of Western Australia and implication for evolution of the supercontinent Columbia. Geoscience Frontiers 3, 241-267.

Moores, E.M., 1991. Southwest US – East Antarctic (SWEAT) connection: a hypothesis. Geology 19, 425-428.

Morrison, G.W., 1980. Characteristics and tectonic setting of the shoshonite rock association. Lithos 13, 97-108.

Nanda, J.K., Rath, S.C., Behera, S.N., 1998. Alkaline and Ultramafic Magmatism in the Contact Zone between High and Low Grade Terrains: Example from NW Orissa, India: Precambrian Crust in Eastern and Central India, Geological Survey of India Publication, Bhubaneswar, India, pp. 122–130.

Neuvonen, K.J., 1965. Palaeomagnetism of the dike systems in Finland: I. Remanent magnetization of Jotnian olivine dolerites in southwestern Finland. Comptes Rendus de la Société Géologique de Finlande 37, 153– 168.

Neuvonen, K.J., 1966. Palaeomagnetism of the dike systems in Finland: II. Remanent magnetization of dolerites in the Vaasa archipelago. Comptes Rendus de la Société Géologique de Finlande 38, 275–281.

Neuvonen, K.J., Grundström, L., 1969. Paleomagnetism of the dike systems in Finland, IV. Remanent magnetization of the dolerite and related dikes in the ? Land archipelago. Bulletin of the Geological Society of Finland 41, 57– 63.

Nilsson, M.K.M, Klausen, M.B., Söderlund, U., Ernst, R.E., 2012. Precise U-Pb ages and geochemistry of Paleoproterozoic mafic dykes from southern West Greenland: Linking the North Atlantic and the Dharwar Cratons. This issue.

Ovchinnikova, G.V., Semikhatov, M.A., Vasil'eva, I.M., Gorokhov, I.M., Kaurova, O.K., Podkovyrov, V.N., Gorokhovskii, B.M., 2001. Pb–Pb age of limestones of the middle Riphean Malgina Formation, the Uchur –Maya region of East Siberia. StratigrAphy and Geological Correlation 9, 490–502.

Pavlov, V.E., Gallet, Y., Shatsillo, A.V., 2000. Palaeomagnetism of the upper Riphean Lakhanda Group of the Uchur–Maya area and the hypothesis of the late Proterozoic supercontinent. Izvestia Fizika Zemli 8, 23– 34 (in Russian).

Pe-Piper, G., Piper, D.J.W., Koukouvelas, I., Dolansky, L.M., Kokkalas, S., 2009. Postorogenic shoshonitic rocks and their origin by melting underplated basalts: The Miocene of Limnos, Greece. Geological Society of America Bulletin 121(1-2), 39-54.

Peccerillo, A., Taylor, S.R., 1976. Geochemistry of eocene calc-alkaline volcanic rocks from the Kastamonu area, Northern Turkey. Contributions to Mineralogy and Petrology 58(1), 63-81.

Pesonen, L.J., Elming, S.-A., Mertanen, S., Pisarevsky, S.A., D'Agrella-Filho, M.S., Meert, J., Schmidt, P.W., Abrahamsen, N., Bylund, G., 2003. Palaeomagnetic configuration of continents during the Proterozoic. Tectonophysics 375, 289-324.

Piper, J.D.A., 1977. Palaeomagnetism of the giant dykes of Tugtutoq and Narssaq Gabbro, Gardar Igneous Province, South Greenland. Bulletin of the Geological Society of Denmark 26, 85-94.

Piper, J.D.A., 1992. The palaeomagnetism of major (Middle Proterozoic) igneous complexes, South Greenland and the Gardar apparent polar wander track. Precambrian Research 54, 153-172.

Pisarevsky, S.A., 2005. New edition of the Global Paleomagnetic Database. EOS transactions, 86(17), 170.

Pisarevsky, S.A., Bylund, G., 2010. Paleomagnetism of 1780-1770 Ma mafic and composite intrusions of Småland (Sweden): implications for the Mesoproterozoic supercontinent. American Journal of Science 310, 1168-1186.

Pisarevsky, S.A., Natapov, L.M., 2003. Siberia and Rodinia. Tectonophysics 375, 221-245.

Pisarevsky, S.A., Wingate, M.T.D., Harris, L.B., 2003. Late Mesoproterozoic (ca 1.2 Ga) palaeomagnetism of the Albany-Fraser orogen: no pre-Rodinia Australia-Laurentia connection. Geophysical Journal International 155, F6-F11.

Pisarevsky, S.A., Natapov, L.M., Donskaya, T.V., Gladkochub, D.P., Vernikovsky, V.A., 2008. Proterozoic Siberia: a promontory of Rodinia. Precambrian Research 160, 66-76.

Polat, A., Hofmann, A.W., 2003. Alteration and geochemical patterns in the 3.7–3.8 Ga Isua greenstone belt, West Greenland. Precambrian Research126, 197-218.

Polat, A., Appel, P.W.U., Fryer, B.J., 2011. An overview of the geochemistry of Eoarchean to Mesoarchean ultramafic to mafic volcanic rocks, SW Greenland: Implications for mantle depletion and petrogenetic processes at subduction zones in the early Earth. Gondwana Research 20, 255-283.

Polat, A., Fryer, B.J., Samson, I.M., Weisener, C., Appel, P.W.U., Frei, R., Windley, B.F., 2012. Geochemistry of ultramafic rocks and hornblendite veins in the Fiskenæsset layered anorthosite complex, SW Greenland: Evidence for hydrous upper mantle in the Archean. Precambrian Research (in press). Poprawa, P., Pacześna, J., 2002. Late Neoproterozoic to Early Palaeozoic development of a rift at the Lublin-Podlasie slope of the East European Craton – analysis of subsidence and facies record (eastern Poland). Przeglad Geologiczny 50(1), 49-63 (in Polish).

Pradhan, V.R., Pandit, M.K., Meert, J.G., 2008. A cautionary note of the age of the paleomagnetic pole obtained from the Harohalli dyke swarms, Dharwar craton, southern India. In: Srivastava, R.K., Sivaji, Ch., Chalapati Rao, N.V. (Eds.), Indian Dykes: Geochemistry, Geophysics, and Geochronology. Narosa Publishing Ltd., New Delhi, India, pp. 339–352.

Pradhan, V.R., Meert, J.G., Pandit, M.K., Kamenov, G., Gregory, L.C., Malone, 1479 S., 2010. India's changing place in global Proterozoic reconstructions: new geochronologic constraints on key paleomagnetic poles from the Dharwar and Aravalli/Bundelkhand Cratons. Journal of Geodynamics 50, 224-242.

Pradhan, V.R., Meert, J.G., Pandit, M.K., Kamenov, G., Mondal, M.E.A., 2012. Paleomagnetic and geochronological studies of the mafic dyke swarms of Bundelkhand craton, central India: implications for the tectonic evolution and paleogeographic reconstructions. Precambrian Research 198-199, 51-76.

Pullaiah, G., Irving, E., Buchan, K.L., Dunlop, D.J., 1975. Magnetisation changes caused by burial and uplift. Earth and Planetary Science Letters 28, 133–143.

Rajesh, H. M., Mukhopadhyay, J., Beukes, N. J., Gutzmer, J., Belyanin, G. A., Armstrong, R. A. 2009. Evidence for an Early Archaean granite from Bastar craton, India. Journal of the Geological Society 166, 193–6.

Ratre, K., De Waele, B., Biswal, T.K., Sinha, S., 2010. SHRIMP geochronology for the 1450 Ma Lakhna dyke swarm: Its implication for the presence of Eoarchaean crust in the Bastar Craton and 1450–517 Ma depositional age for Purana basin (Khariar), Eastern Indian Peninsula. Journal of Asian Earth Sciences 39, 565-577.

Rickers, K., Mezger, K., Raith, M., 2001. Evolution of the continental crust in the Proterozoic Eastern Ghats Belt, India and new constraints for Rodinia reconstruction: implications from Sm–Nd, Rb–Sr and Pb–Pb isotopes. Precambrian Res. 112, 183– 210.

Rogers, J.W.J., Santosh, M., 2002. Configuration of Columbia, a Mesoproterozoic Supercontinent. Gondwana Research 5, 5-22.

Rogers, J.J.W., Santosh, M., 2009. Tectonics and surface effects of the supercontinent Columbia. Gondwana Research 15, 373–380.

Rosen, O.M., Condie, K.C., Natapov, L.M., Nozhkin, A.D., 1994. Archean and Early Proterozoic evolution of the Siberian craton: a preliminary assessment. In: Condie, K.C. (Ed.), Archean Crustal Evolution. Elsevier, Amsterdam, pp. 411–459.

Ross, G.M., Bloch, J.D., Krouse, H.R., 1995. Neoproterozoic strata of the southern Canadian Cordillera and the isotopic evolution of seawater sulfate. Precambrian Research 73, 71-99.

Roy, A., Prasad, M.H., 2003. Tectonothermal events in Central Indian Tectonic Zone (CITZ) and its implications in Rodinian crustal assembly. Journal of Asian Earth Sciences 22, 115-129.

Roy, A., Kagami, H., Yoshida, M., Roy, A., Bandyopadhyay, B.K., Chattopadhyay, A., 2006. Rb/Sr and Sm/Nd dating of different metamorphic events from the Sausar mobile belt, central India; implications for Proterozoic crustal evolution. Journal of Asian Earth Sciences 26, 61–76.

Roy, J. L., Robertson, W. A., 1978. Paleomagnetism of the Jacobsville Formation and the apparent polar path for the interval -1100 to -670 m.y. for North America. Journal of Geophysical Research 83,1289-1304.

Salminen, J., Pesonen, L.J., 2007. Paleomagnetic and rock magnetic study of the Mesoproterozoic sill, Valaam island, Russian Karelia. Precambrian Research 159, 212-230.

Salminen, J., Pesonen, L.J., Mertanen, S., Vuollo, J., Airo, M.-L., 2009. Palaeomagnetism of the Salla Diabase Dyke, northeastern Finland, and its implication for the Baltica–Laurentia entity during the Mesoproterozoic. In: Reddy, S. M., Mazumder, R., Evans, D. A. D., Collins, A. S. (eds), Palaeoproterozoic Supercontinents and Global Evolution. Geological Society, London, Special Publications, vol. 323, pp.199–217.

Santosh, M., 2012. India's Palaeoproterozoic legacy. Geological Society of London Special Publications, vol. 365, p. 263-288

Sarkar, G., Corfu, F., Paul, D.K., McNaughton, N.J., Gupta, S.N., Bishui, P.K., 1993. Early Archean crust in Bastar craton, central India – a geochemical and isotopic study. Precambrian Research 62, 127–137.

Scarrow, J.H., Bea, F., Montero, P., Molina, J.F., 2008. Shoshonites, vaugnerites and potassic lamprophyres: similarities and differences between 'ultra'-high-K rocks. Earth and Environmental Science Transactions of the Royal Society of Edinburgh 99, 159-175.

Schofield, D.I., Thomas, R.J., Goodenough, K.M., De Waele, B., Pitfield, P.E.J., Key, R.M., Bauer, W., Walsh, G.J., Lidke, D.J., Ralison, A.V., Rabarimanana, M., Rafahatelo, J.M., Randriamananjara, T., 2010. Geological evolution of the Antongil Craton, NE Madagascar. Precambrian Research 182, 187-203.

Sears, J.W., Price, R.A., 2000. New look at the Siberian connection: no SWEAT. Geology 28, 423-426.

Shchipansky, A.A., Bogdanova, S.V., 1996. The Sarmatian crustal segment: Precambrian correlation between the Voronezh Massif and the Ukrainian Shield across the Dniepr-Donets aulocogen. Tectonophysics 268, 109-125.

Shchipansky, A.A., Samsonov, A.V., Petrova, A.Y., Larionova, Y.O., 2007. Geodynamics of the Eastern Margin of Sarmatia in the Paleoproterozoic. Geotectonics 41 (1), 38–62.

Söderlund, U. and Johansson, L., 2002. A simple way to extract baddeleyite (ZrO_2). Geochemistry Geophysics Geosystems, 3(2), doi: 10.1029/2001GC000212.

Srivastava, R.K., 2006. Precambrian mafic dyke swarms from the central Indian Bastar craton: Temporal evolution of the subcontinental mantle. In: Hanski, E., Mertanen, S., Rämö, T., Vuollo, J. (Eds), Dyke swarms – time markers of crustal evolution. Taylor & Francis Group, London, ISBN 0 415 39899 1, pp.147-159.

Srivastava, R.K., Singh, R.K., Verma, S.P., 2004. Neoarchaean mafic volcanic rocks from the southern Bastar greenstone belt, Central India: petrological and tectonic significance. Precambrian Research 131, 305-322.

Stearn, J. E. F., Piper, J. D. A., 1984. Palaeomagnetism of the Sveconorwegian mobile belt of the Fennoscandian Shield. Precambrian Research 23, 201–246, doi: 10.1016/0301-9268(84)90045-7.

Stein, H.J., Hannah, J.L., Zimmerman, A., Markey, R.J., Sarkar, S.C., Pal, A.B., 2004. A 2.5 Ga porphyry Cu–Mo–Au deposit at Malanjkhand, central India; implications for late Archean continental assembly. Precambrian Research 134, 189–226.

Sun, S.S., McDonough, W.F., 1989. Chemical and isotope systematics of oceanic basalts: implication for mantle composition and processes. In: Saunders,A.D., Norry,M.J.(Eds), Magmatism in the Ocean Basins, Geological Society Special Publication 42, 313-345.

Tucker, R.D., Ashwal, L.D., Torsvik, T.H., 2001. U-Pb geochronology of Seychelles granitoids: a Neoproterozoic continental arc fragment. Earth and Planetary Science Letters 187, 27-38.

Upton, B.G.J., Emeleus, C.H., Heaman, L.M., Goodenough, K.M., Finch, A.A., 2003. Magmatism of the mid-Proterozoic Gardar Province, South Greenland: chronology, petrogenesis and geological setting. Lithos 68, 43-65.

Walton,D., 1980. Time-temperature relations in the magnetisation of assembles of single-domain grains. Nature 286, 245–247.

Wang, X.-C., Li, X.-H., Li, W.-X, Li, Z.X. Liu, Y., Yang, Y.-H., Liang, X.-R., Tu, X.-L., 2008. The Bikou basalts in the northwestern Yangtze block, South China: Remnants of 820-810 Ma continental flood basalts? Geological Society of America Bulletin 120(11-12), 1478-1492.

Wang, X.-C., Li, X.-H., Li, Z.-X., Liu, Y., Yang, Y.-H., 2010. The Willouran basic province of South Australia: Its relation to the Guibei large igneous province in South China and the breakup of Rodinia. Lithos 119(3-4), 569-584.

Warnock, A.C., Kodama, K.P., Zeitler, P.K., 2000. Using thermochronometry and low-temperature demagnetization to accurately date Precambrian paleomagnetic poles. Journal of Geophysical Research 105, 19435-19453.

Weil, A.B., Geissman, J.W., Heizler, M., Van der Voo, R., 2003. Paleomagnetism of Middle Proterozoic mafic intrusions and Upper Proterozoic (Nankoweap) red beds from the Lower Grand Canyon Supergroup, Arisona. Tectonophysics 375, 199-220.

Wingate, M. T. D., Pisarevsky, S. A., Evans, D. A. D., 2002. A revised Rodinia supercontinent: no SWEAT, no AUSWUS. Terra Nova 14, 121-128.

Wingate, M.T.D., Pisarevsky, S.A., Gladkochub, D.P., Donskaya, T.V., Konstantinov, K.M., Mazukabzov, A.M., Stanevich, A.M., 2009. Geochronology and paleomagnetism of mafic igneous rocks in the Olenek Uplift, northern Siberia: implications for Mesoproterozoic supercontinents and paleogeography. Precambrian Research 170, 256-266.

Yedekar, D.B., Jain, S.C., Nair, K.K.K., Dutta, K.K., 1990. The central Indian collision suture, Precambrian of Central India. Geological Society of India Special Publication 57, 9-25.

Zartman, R.E., Nicholson, S.W., Cannon, W.F., Morey, G.B., 1997. U-Th-Pb zircon ages of some Keweenawan Supergroup rocks from the south shore of Lake Superior. Canadian Journal of Earth Sciences 34, 549-567.

Zhao, G., Sun, M., Wilde, S.A., Li, S., 2004 A Paleo-Mesoproterozoic supercontinent: assembly, growth and breakup. Earth-Science Reviews 67, 91–123.

Figure captions

Fig. 1. (a) Location and geological province map of India (geology based on, Commission for the Geological Map of the World, 2000); (b) Geological map of the Lakhna area and sampling sites. The cross-section is approximately along 20°40' 30" N.

Fig. 2. Photomicrographs in transmitted (a-d) and reflected (e-h) light: (a) rhyolite showing quartz (Q) and feldsdpar phenocrysts (Or) in a fine to medium grained quartzofeldspathic groundmass; (b) trachyte with single or multiple feldspars phenocrysts (Or-Orthoclase, Plg- Plagioclase); (c) dolerite

showing augite (Px) (colored mineral) and plagioclase (Plg) (white and grey shade) crystals with irregular grain margin; (d) alkali gabbro showing intergrowth between alkali (Or) and plagioclase feldspars (Plg); magnetite (Mag) with martite (Mar) minerals of the different dyke sections (e) dolerite (DL6-D2); (f) trachyte (DL7B-D10); (g) rhyolite porphyry (MA1); (h) rhyolite porphyry with higher magnification (MA1).

Fig. 3. Analysis of Curie points using magnetic susceptibility versus temperature curves.

Fig. 4. Stereoplots and examples of demagnetisation behaviour for studied dykes. In orthogonal plots, open (closed) symbols show magnetisation vector endpoints in the vertical (horizontal) plane; curves show changes in intensity during demagnetisation. Stereoplots show upwards (downwards) pointing palaeomagnetic directions with open (closed) symbols. (a) rhyolite; (b) dolerite; (c) trachytes.

Fig. 5. Stereoplots of the site mean palaeomagnetic directions. (a) 10 dykes; (b) 8 dykes (D4 and D8 are excluded.

Fig. 6. Representative zircon grains, and fragments, extracted from the sample D5. Upper image (optical microscope) shows prismatic grains with sharp edges between crystal surfaces (black arrows). Most grains have abundant fractures but are crystalline with no signs of radiation damage. Lower image (back-scattered electron image) shows two grains with no internal zoning, overgrowth or internal older components (cores). Some of the fractures probably stem from the polishing. White arrows depict sharp edges between crystal surfaces.

Fig. 7. U-Pb Concordia diagram for the Lakhna sample D5. Dark grey ellipse defines the Concordia age for fraction Z1 and Z2. Ellipses depict 2s error.

Fig. 8. (a) Total alkalis vs. SiO_2 diagram for the classification of the Lakhna dykes (Le Bas et al., 1986); (b) the shoshonite diagram of Peccerillo and Taylor (1976). Filled and open circles represent the alkalic series (Group 1 in Tables 3,4) and the sub-alkalic series (Group 2 in Tables 3,4) respectively. Red symbols denote samples analysed by ICP-MS at ACME Labs in Canada, blue symbols were analysed by ICP-AES at the Indian Institute of Technology, Bombay.

Fig. 9. REE-chondrite normalised patterns for (1) mafic dykes of Group 1; (2) mafic dykes of Group 2; (3) andesitic dykes; (4) dacite to rhyolite dykes. Normalisation values are from Sun and McDonough (1989). The solid and dashed lines indicate Group 1 and Group 2, respectively.

Fig. 10. Primitive mantle-normalised incompatible trace element spidergrams for the (1) mafic dykes of Group1; (2) mafic dykes of Group 2; (3) andesitic dykes; (4) dacite to rhyolite dykes. Normalisation values are from Sun and McDonough (1989). The solid and dashed lines indicate Group-1 and Group-2, respectively.

Fig. 11. Nb/La, Th/La and La/Yb versus SiO_2 and MgO. Filled and open circles represent the alkalic series (Group 1 in Tables 3, 4) and the sub-alkalic series (Group 2 in Tables 3, 4) respectively.

Fig. 12. Palaeomagnetically permissive 1460 Ma reconstructions of India (I) juxtaposed to: (a) SE Laurentia (L); (b) SW Laurentia; (c) SW Siberia (S); (d) SW Baltica (B) - Sarmatia. Hereafter: circles – Baltican poles; triangles – Laurentian poles; squares – Siberian poles; diamonds – Indian poles. Insets show geological matches/mismatches for each reconstruction. TIB - Transscandinavian Igneous Belt; GO - Gothian Orogeny; TA - Telemarkian accretionary events; DPO - Hallandian-Danopolonian orogeny; SNO - Sveconorwegian orogeny. Kimberlites and lamproites are located after Chalapathi Rao et al. (2004), Kumar et al. (2007), Bogatikov et al. (2007). Laurentian and Indian palaeopoles rotated together with continents (Table 6). Euler rotation parameters for India – see figure caption 13.

Fig. 13. Palaeomagnetic testing of: (a) the India-SE Laurentia fit (Fig. 12a) at ~1190 Ma and ~1080 Ma (India is rotated to Laurentia about an Euler pole of 16.01°S, 7.90°W at 136.28° anticlockwise); (b) the India-SW Laurentia fit (Fig. 12b) at ~1190 Ma and ~1080 Ma (India is rotated to Laurentia about an Euler pole of 8.73°N, 20.68°W at 106.10° anticlockwise); (c) the India-SW Siberia fit (Fig. 12c) at ~1190 Ma and ~1080 Ma (India is rotated to Siberia about an Euler pole of 28.63°N, 93.94°E at 129.84° clockwise); (d) the India-SW Baltica fit (Fig. 12d) at ~1120 Ma and ~1080 Ma (India is rotated to Baltica about an Euler pole of 30.67°N, 54.34°E at 184.93° clockwise)..

Online appendixes

Appendix A: Plots of major and selected trace elements against SiO_2. Symbology as in Fig. 8.

Appendix B: Na_2O and K_2O versus LOI and Zr. Filled and circles represent the alkalic series (Group1 in Tables 3 and 4) and the sub-alkalic series (Group 2 in Tables 3 and 4) respectively.

Appendix C: Standard data and average value of samples analysed in laboratory in IIT Bombay (JSY-1, JG, JR-3, JG2 and JG1a) and in ACME Ltd (SO-18).

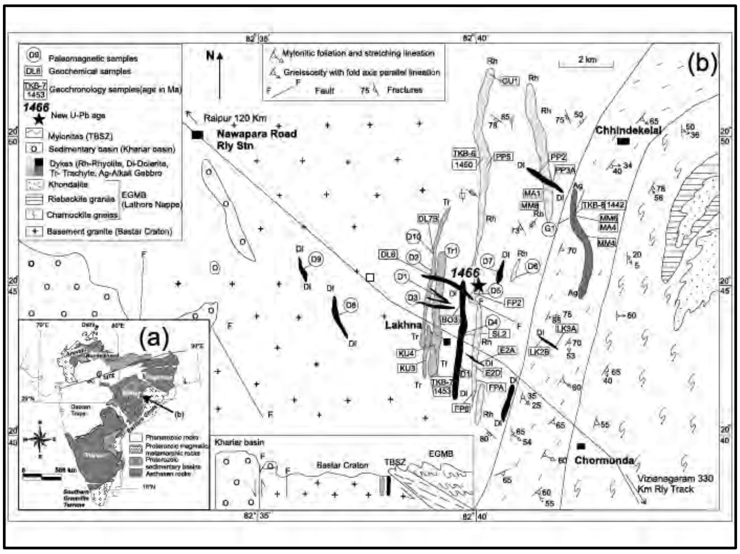

Figure 1

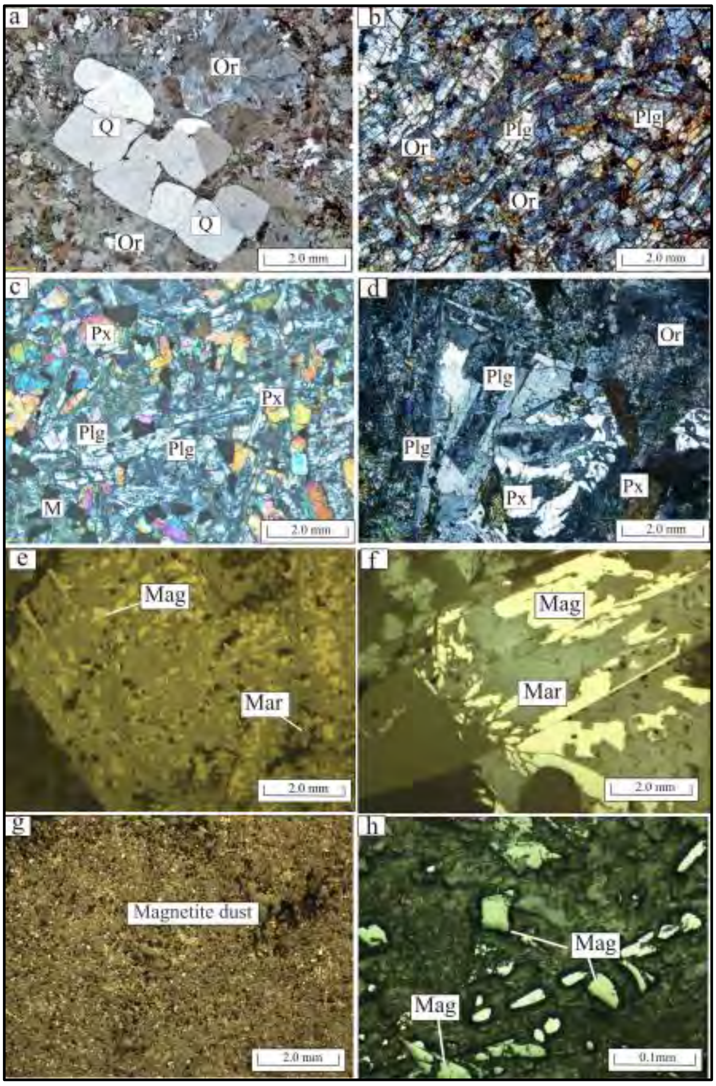

Figure 2

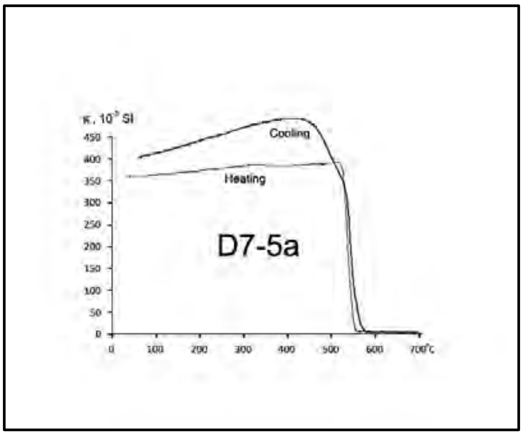

Figure 3

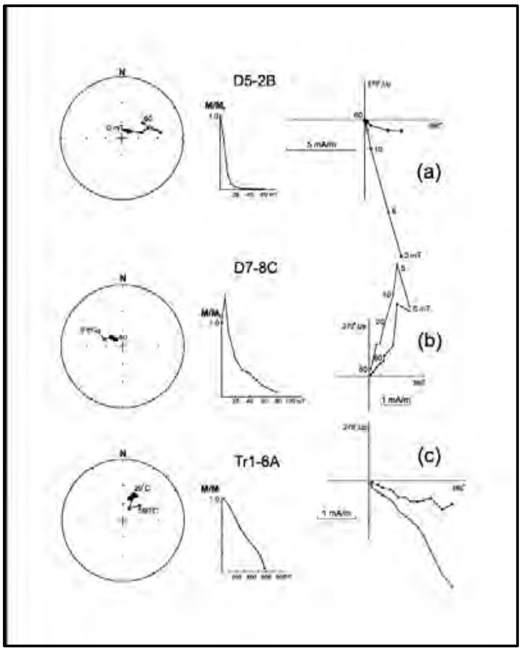

Figure 4

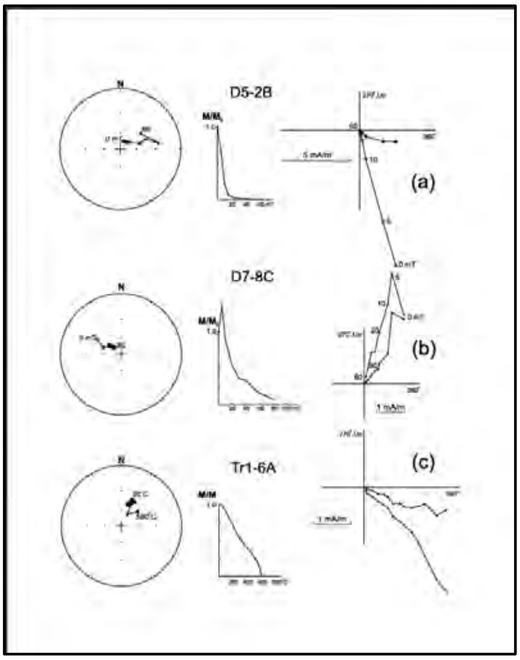

Figure 5

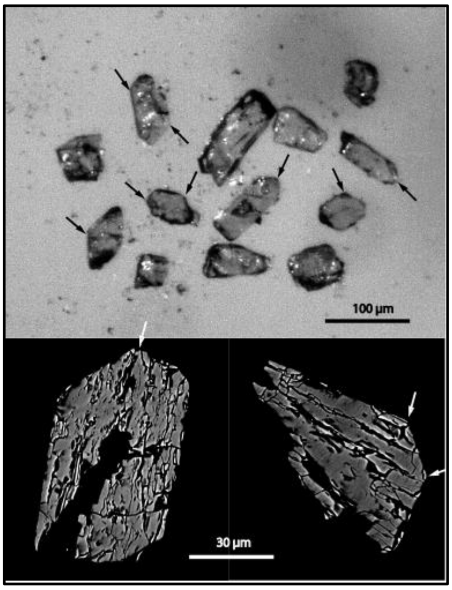

Figure 6

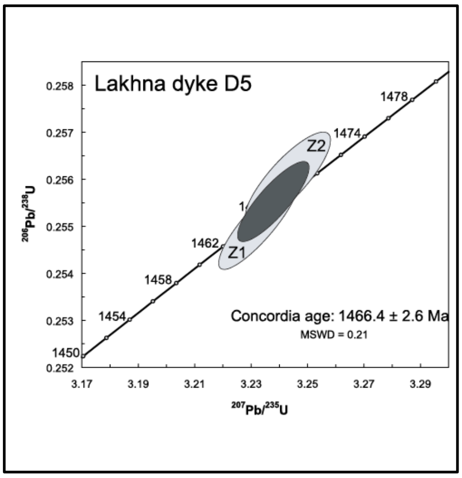

Figure 7

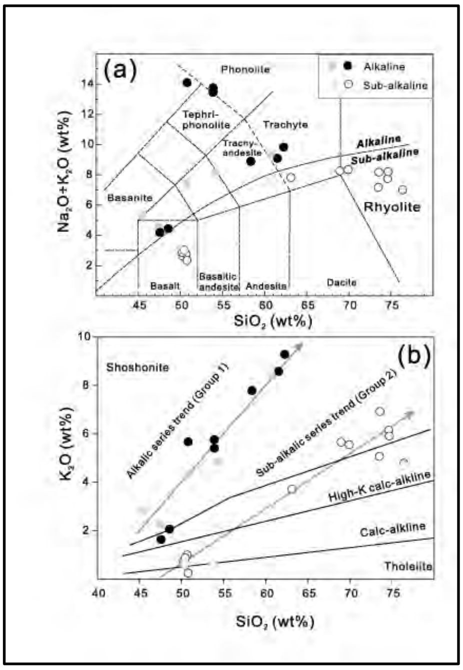

Figure 8

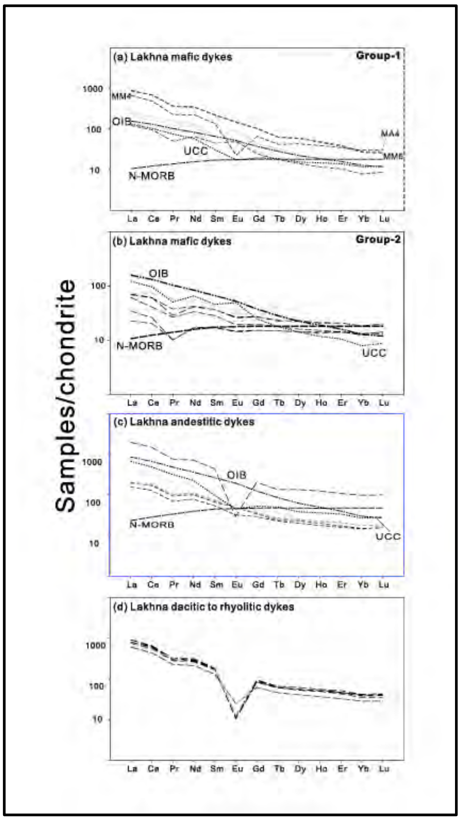

Figure 9

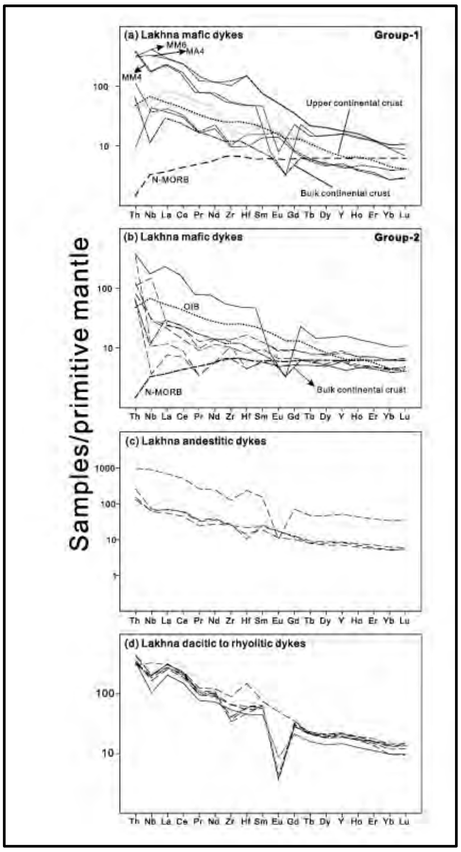

Figure 10

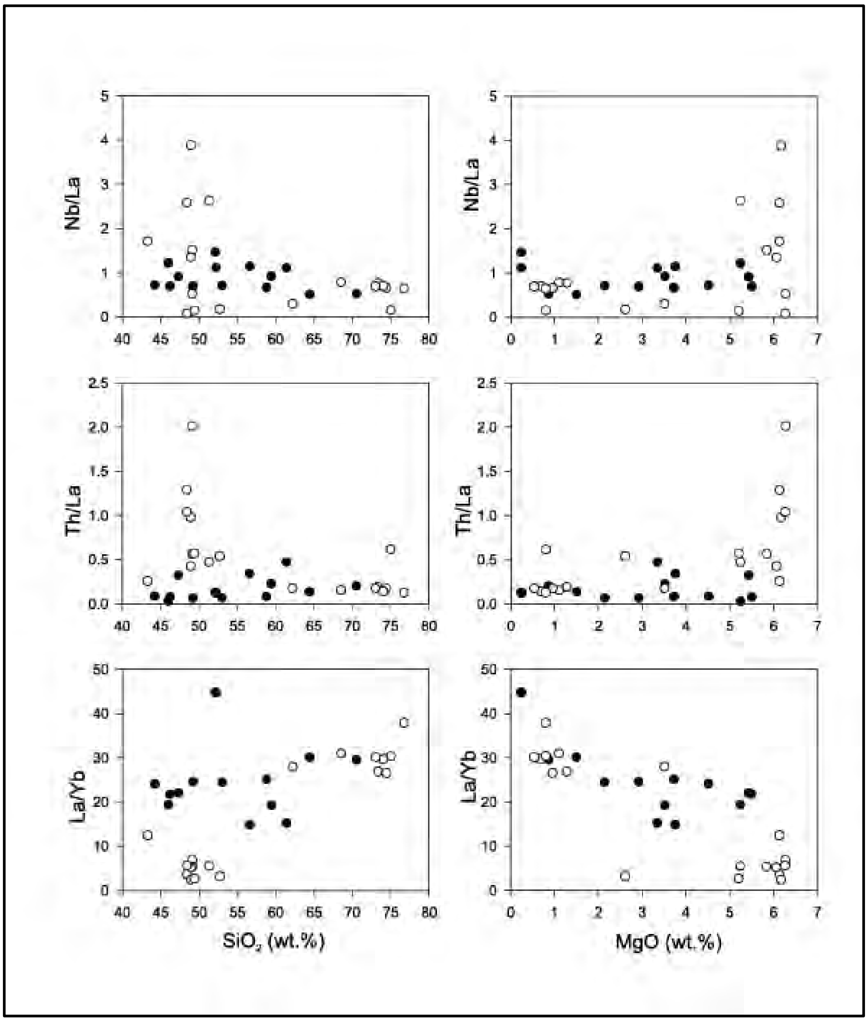

Figure 11

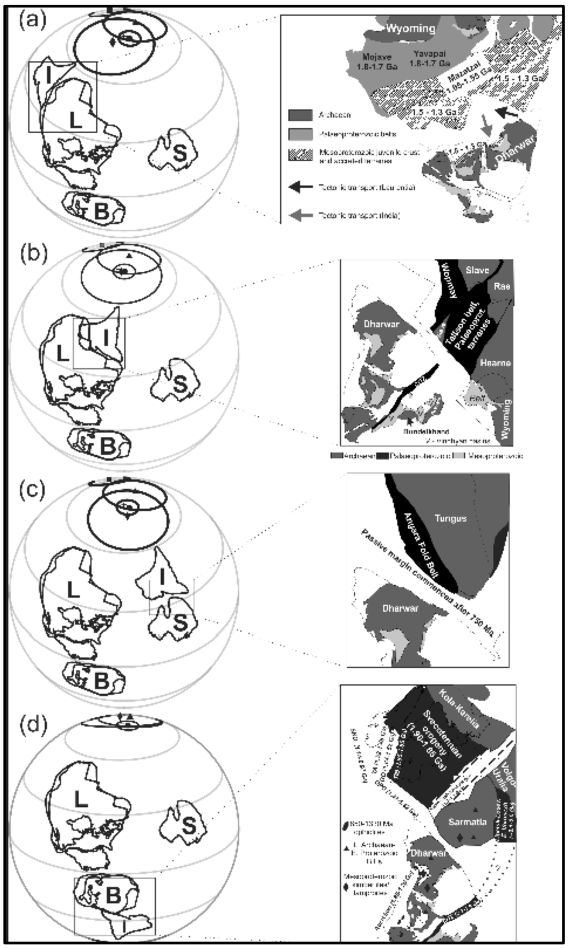

Figure 12

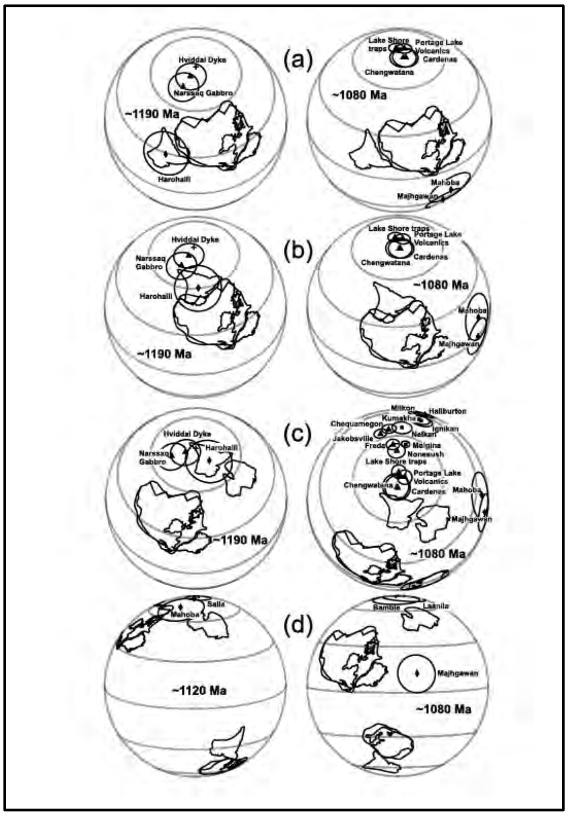

Figure 13

Table 1. Paleomagnetic directions of Lakhna dykes

#	Location N	E	n/N	D (°)	I (°)	K	α_{95} (°)	Plat (°N)	Plong (°E)	dp (°)	dm (°)
D1	20°44.957'	82°38.951'	10/13	50.6	58.4	19.1	11.4	43.2	137.9	12.5	16.9
D2	20°45.086'	82°39.001'	4/4	96.0	61.6	43.4	14.1	9.7	130.4	16.8	21.8
D3	20°44.890'	82°38.937'	10/16	57.1	59.5	11.0	15.3	38.1	137.0	17.3	23.0
D4	20°43.981'	82°39.520'	6/11	338.5	67.1	21.2	14.9	56.3	57.4	20.5	24.7
D5	20°45.114'	82°39.853'	7/9	64.9	56.6	19.0	14.2	32.0	141.0	14.9	20.6
D6	20°45.534'	82°40.810'	5/5	42.2	55.1	48.6	11.1	50.3	141.4	11.2	15.8
D7	20°45.533'	82°40.341'	6/9	293.6	-67.0	31.7	12.1	1.6	119.1	16.6	20.0
D8	20°44.360'	82°36.596'	6/8	93.8	-67.6	24.2	13.9	17.9	40.7	19.4	23.2
D10	20°45.153'	82°38.924'	14/18	51.7	65.2	17.8	9.7	40.8	127.4	12.7	15.7
Tr1	20°43.840'	82°38.785'	11/12	19.7	54.7	38.8	7.4	67.2	127.7	7.4	10.5
All mean			10/79	48.5	68.7	14.4	13.2	41.3	120.5	18.9	22.3
Mean without D4,D8			8/60	58.7	62.5	30.7	10.2	36.6	132.8	12.4	15.9

N/n=number of samples/specimens; D, I=sample mean declination, inclination;

k =best estimate of the precision parameter of Fisher (1953);

α_{95}= the semi-angle of the 95% cone of confidence;

Plat, Plong = latitude, longitude of the palaeopole;

dp ,dm =the semi-axes of the cone of confidence about the pole at the 95% probability level.

Table 2. U-Pb TIMS data

Analysis no. (number of grains)	U/ Th	Pbc/ Pbtot[1)]	$^{206}Pb/^{204}Pb$ raw[2)]	$^{207}Pb/^{235}U$ [corr][3)]	± 2s % err	$^{206}Pb/^{238}U$	± 2s % err	$^{207}Pb/^{235}U$ [age, Ma]	$^{206}Pb/^{238}U$	$^{207}Pb/^{206}Pb$	± 2s	Concord-ance
Z1 (3 grains)	1.2	0.027	1892.9	3.2329	0.32	0.25509	0.27	1465.1	1464.7	1465.7	3.3	0.999
Z2 (3 grains)	1.3	0.026	1964.7	3.2427	0.38	0.25602	0.31	1467.4	1469.4	1464.6	4.1	1.003

1) Pbc = common Pb; Pbtot = total Pb (radiogenic + blank + initial).

2) measured ratio, corrected for fractionation and spike.

3) isotopic ratios corrected for fractionation (0.1% per amu for Pb), spike contribution, blank (1 pg Pb and 0.1 pg U), and initial common Pb. Initial common Pb corrected with isotopic compositions from the model of Stacey and Kramers (1975) at the age of the sample.

Table 3. Major and trace elements (Canada)

Sample	Sample 1	Sample 2	Sample 3	Sample 4	Sample 5	Sample 6	Sample 7	Sample 8	Sample 9	Sample 10
Dyke # (palaeomag)	D1	D2	D3	D4	D5	D6	D7	D8	D9	D10
Group	1.00	2.00	1.00	1.00	2.00	1.00	1.00	2.00	2.00	1.00
Major elements (%)										
SiO_2	49.2	48.4	53.0	46.2	75.0	64.4	44.2	49.4	52.7	58.8
TiO_2	2.72	2.18	2.06	2.96	0.250	0.790	3.83	1.38	1.49	1.05
Al_2O_3	14.4	13.0	14.8	14.3	12.1	14.8	13.8	13.6	14.4	15.6
$Fe_2O_{3\ total}$	13.0	15.2	11.7	14.2	2.36	6.48	16.3	16.0	15.3	7.37
MgO	2.92	6.26	2.14	5.50	0.800	1.50	4.51	5.20	2.61	3.72
CaO	5.87	9.58	4.93	8.68	0.380	0.850	7.81	9.11	7.46	0.910
Na_2O	3.06	2.17	3.24	2.21	2.56	3.79	2.42	2.31	3.00	0.840
K_2O	4.19	0.860	4.74	2.19	4.60	4.73	2.77	0.620	0.610	8.19
P_2O_5	1.23	0.260	0.950	0.930	0.0300	0.230	1.34	0.170	0.290	0.320
MnO	0.230	0.230	0.210	0.190	<0.01	0.0900	0.220	0.210	0.190	0.0600
Cr_2O_3	<0.002	0.0190	<0.002	0.0130	<0.002	<0.002	<0.002	0.0110	0.00300	<0.002
LOI	2.40	1.50	1.60	2.00	1.40	2.00	2.20	1.60	1.70	2.80
Sum	99.3	99.6	99.4	99.4	99.6	99.7	99.4	99.7	99.8	99.7
Trace elements (ppm)										
Be	1.00	<1	<1	<1	2.00	3.00	2.00	<1	<1	<1
Sc	23.0	47.0	21.0	29.0	<1	7.00	26.0	39.0	28.0	19.0
V	98.0	373	40.0	274	<8	20.0	242	361	161	<8
Co	53.2	57.3	24.4	52.9	32.6	24.0	53.4	63.5	52.9	9.10
Ni	7.00	29.6	3.70	37.8	2.60	6.20	15.2	24.4	10.7	2.10
Cu	13.9	64.0	8.40	51.1	0.900	11.1	20.4	178	83.7	1.40
Zn	94.0	72.0	83.0	65.0	44.0	118	96.0	48.0	77.0	65.0
Ga	19.8	19.2	19.5	17.3	27.7	30.7	19.1	18.6	19.9	22.6
As	0.900	0.900	<0.5	0.600	0.700	0.700	1.60	<0.5	<0.5	0.600
Se	<0.5	<0.5	<0.5	<0.5	1.00	<0.5	<0.5	<0.5	<0.5	<0.5
Rb	71.4	35.7	84.3	95.6	154	167	71.0	25.9	19.7	213
Sr	606	282	593	780	14.4	80.2	796	141	163	41.4
Y	30.3	36.0	30.6	20.6	99.8	58.4	25.5	33.0	52.4	38.1
Zr	206	150	247	116	823	565	177	108	220	307
Nb	38.4	19.7	41.9	22.4	157	77.1	32.4	5.10	9.20	59.1
Mo	1.00	0.700	1.10	0.500	0.800	2.40	0.800	0.500	0.600	1.70
Ag	<0.1	0.100	0.100	0.100	<0.1	0.200	0.100	<0.1	<0.1	<0.1
Cd	<0.1	<0.1	<0.1	<0.1	<0.1	0.100	<0.1	0.100	0.100	<0.1
Sn	1.00	2.00	<1	<1	6.00	7.00	<1	1.00	2.00	2.00
Sb	<0.1	<0.1	<0.1	<0.1	<0.1	<0.1	<0.1	<0.1	<0.1	<0.1
Cs	0.800	0.400	1.30	1.30	0.600	0.200	0.500	0.100	0.200	0.400
Ba	3793	383	3583	2287	127	520	2314	199	293	1029
La	55.3	18.9	59.0	32.2	254	151	44.8	8.90	17.0	88.7
Ce	123	43.9	129	72.4	506	315	103	22.3	43.8	190
Pr	14.2	5.34	15.0	8.38	50.3	30.9	11.8	2.83	5.39	19.8
Nd	59.4	23.4	63.4	39.0	184	110	50.9	13.8	26.2	74.5
Sm	10.6	5.36	10.4	6.63	28.4	16.5	9.28	3.92	6.35	11.7
Eu	5.41	1.77	5.59	3.29	0.720	1.45	4.33	1.27	2.05	3.36
Gd	8.97	6.21	8.69	5.55	22.3	11.7	7.89	4.81	7.98	8.62
Tb	1.22	1.08	1.25	0.800	3.48	1.93	1.11	0.890	1.46	1.34
Dy	6.23	6.53	6.05	4.11	18.7	9.84	5.43	5.29	8.67	7.07
Ho	1.00	1.21	1.03	0.700	3.36	1.84	0.910	1.15	1.84	1.29
Er	2.67	3.51	2.89	1.75	9.16	5.34	2.18	3.51	5.43	3.45
Tm	0.390	0.570	0.430	0.290	1.44	0.910	0.370	0.540	0.890	0.580
Yb	2.25	3.35	2.41	1.48	8.36	5.01	1.86	3.33	5.34	3.53
Lu	0.350	0.550	0.390	0.230	1.26	0.780	0.310	0.540	0.830	0.560
Hf	4.60	4.50	6.10	3.00	23.6	13.7	4.80	2.50	5.70	7.40

Ta	2.40	1.20	2.50	1.30	9.10	4.70	2.40	0.400	0.800	3.60
W	79.7	86.3	84.4	53.2	357	167	68.2	112	172	58.4
Au	3.80	3.00	4.50	1.80	1.90	2.00	1.00	3.50	2.50	1.60
Hg	<0.01	<0.01	0.0200	<0.01	<0.01	0.0200	<0.01	0.0200	0.0200	<0.01
Tl	<0.1	<0.1	<0.1	0.200	0.200	0.200	<0.1	<0.1	<0.1	<0.1
Pb	1.90	1.30	2.40	1.50	4.30	23.4	2.40	0.800	1.50	2.40
Bi	<0.1	<0.1	<0.1	<0.1	<0.1	<0.1	<0.1	<0.1	<0.1	<0.1
Th	3.70	1.60	4.00	2.50	39.8	21.1	3.90	1.30	3.00	7.50
U	0.700	0.500	0.700	0.500	5.50	3.30	0.700	0.400	0.800	1.80

Table 4. Major and trace elements (India)

Sample:	MM6	MM4	MM8	MA1	PP3A	GU1	PP5	KU3	KU4	PP2	LK2B	SL2	E2A	E2D	DL6	DL7B	FP6	FPA	FP2	BO3	LK-3A	D1
Dyke # (palaeomag)	G1	G1				D5	D5	Tr1	Tr1			D4	D5	D5	D2	D10	D5	D5	D5	D4		D4
Group	1.00	1.00	1.00	2.00	2.00	2.00	2.00	1.00	1.00	2.00	1.00	1.00	2.00	2.00	2.00	1.00	2.00	2.00	2.00	2.00	2.00	2.00
SiO_2	52.1	52.2	70.5	68.5	48.4	73.3	74.4	59.4	61.4	48.9	47.3	46.0	49.1	62.2	49.1	56.6	74.0	73.0	76.7	48.9	43.3	51.3
TiO_2	0.960	0.670	0.460	0.500	1.54	0.290	0.265	1.50	1.54	1.45	3.06	2.80	1.56	0.757	2.18	1.36	0.249	0.337	0.258	2.10	3.57	3.37
Al_2O_3	17.8	18.0	14.6	14.4	13.9	13.1	12.0	16.7	16.1	14.2	15.1	15.4	15.2	16.1	13.3	15.7	12.4	12.9	12.5	13.1	15.3	13.7
$Fe_2O_{3\,total}$	10.0	9.74	5.05	5.50	14.6	3.68	3.54	6.25	6.24	14.0	14.9	14.1	12.9	6.93	15.5	11.1	4.06	4.74	2.81	14.7	15.8	13.4
MgO	0.240	0.240	0.860	1.10	6.13	1.28	0.953	3.52	3.34	6.17	5.43	5.24	6.27	3.51	5.84	3.75	0.686	0.534	0.794	6.06	6.13	5.24
CaO	2.90	3.01	1.18	1.37	9.36	0.120	0.470	0.508	0.470	10.9	7.47	9.40	9.93	1.71	9.83	0.452	0.404	0.997	0.430	9.92	10.0	9.66
Na_2O	7.43	8.08	2.81	2.59	2.07	1.25	2.29	0.495	0.546	1.90	2.33	2.48	1.69	4.05	2.09	1.07	1.58	2.09	2.23	2.02	2.18	2.15
K_2O	5.58	5.24	5.60	5.62	0.847	6.90	5.89	8.30	9.16	0.674	2.01	1.59	0.969	3.67	0.710	7.56	6.10	5.04	4.81	0.241	2.22	0.630
P_2O_5	0.0500	0.0300	0.0700	0.0900	0.0860	0.00900	0.0100	0.302	0.298	0.0730	0.948	0.776	0.172	0.0520	0.278	0.240	0.00100	0.0250	0.00100	0.239	1.10	0.290
MnO	0.350	0.350	0.0600	0.0700	0.202	0.0140	0.0210	0.0260	0.0220	0.229	0.199	0.188	0.211	0.0410	0.247	0.0820	0.0250	0.0430	0.0100	0.227	0.229	0.220
LOI	2.04	1.99	1.14	0.0140	1.84	1.09	1.10	3.23	1.73	1.88	1.77	2.44	2.80	1.74	1.16	2.51	0.720	0.00900	0.00730	2.78	2.06	2.02
Total	99.5	99.5	102	99.7	99.0	101	101	100	101	100	100	100	101	101	100	100	100	99.7	101	100	102	102
Trace element (ppm)																						
Sc	0	0.200	0.300	1.30	9.20	0.200	0	1.10	18.5	11.9	4.85	1.70	9.80	0.200	10.6	7.20	5.40	0	0.400	11.1	9.50	11.0
V	30.0	16.0	12.0	0	196	5.00	0	44.0	58.0	148	271	201	234	17.0	200	51.0	6.00	8.00	6.00	263	208	246
Cr	174	156	420	164	260	494	332	147	156	208	177	255	262	156	262	166	510	498	553	221	147	275
Co	6.00	11.0	3.00	4.00	46.0	1.00	1.00	9.00	14.0	45.0	43.0	46.0	41.0	22.0	45.0	8.00	10.0	1.00	1.00	42.0	42.0	43.0
Ni	12.0	15.0	19.0	21.0	76.0	21.0	22.0	16.0	17.0	85.0	46.0	101	40.0	18.0	43.0	16.0	21.0	21.0	20.0	46.0	42.0	44.0
Rb	134	114	162	159	46.0	213	184	160	181	41.0	70.0	56.0	41.0	202	39.0	159	212	203	187	33.0	49.0	44.0
Sr	2365	2232	54.0	80.0	385	15.0	15.0	59.0	61.0	151	593	674	196	54.0	189	46.0	14.0	20.0	10.0	170	749	223
Y	82.1	86.9	66.8	71.9	28.7	96.1	97.2	36.9	38.7	26.8	21.3	23.2	27.1	230	40.6	31.7	89.0	100	85.4	37.5	23.1	43.1
Zr	1135	1001	607	612	115	745	734	276	291	74.0	114	108	120	1373	153	282	403	459	382	143	40.0	117
Nb	296	235	74.6	124	20.8	148	118	44.4	50.8	20.6	26.1	30.8	7.60	138	25.2	42.6	133	148	142	21.8	27.8	41.6
Cs	13.1	11.5	9.80	8.80	7.50	8.90	12.0	10.2	6.60	10.6	4.30	2.00	4.20	14.0	9.30	5.30	6.70	8.50	11.2	7.80	11.5	9.00
Ba	385	369	579	567	524	305	119	1026	1024	158	2028	1196	224	129	213	706	163	91.0	118	120	1963	282
La	202	210	142	158	8.05	191	178	48.1	45.7	5.30	28.7	25.2	14.4	462	16.6	37.2	190	214	220	16.1	16.2	15.8
Ce	422	419	267	296	15.8	376	334	103	110	12.4	58.2	53.6	24.7	904	37.1	78.5	359	404	383	36.5	37.5	33.5
Pr	33.9	34.7	21.4	21.4	0.900	28.9	26.5	8.90	9.70	1.00	4.70	4.50	2.50	71.3	2.70	6.60	26.9	29.7	31.0	3.50	5.30	3.53
Nd	160	164	99.5	104	7.90	133	122	47.1	51.6	7.70	30.4	26.2	15.5	331	19.0	36.4	127	138	146	19.6	22.5	19.7
Sm	33.8	33.4	19.9	20.7	2.70	28.2	25.5	10.1	11.1	2.50	6.90	6.10	4.30	67.2	5.50	8.20	26.7	28.8	28.2	5.60	5.50	5.32
Eu	8.80	8.30	1.40	1.30	0.800	0.700	0.600	2.80	2.80	0.800	2.80	2.40	1.10	1.70	1.50	1.90	0.600	0.700	0.700	1.50	2.10	1.25

Gd	21.2	20.9	12.7	13.6	3.10	18.3	16.9	7.00	7.50	3.10	5.00	4.80	4.00	41.7	5.60	6.00	16.8	19.4	18.3	5.50	3.00	3.85
Tb	2.40	2.30	1.70	1.50	0.600	2.50	2.30	0.900	1.00	0.600	0.700	0.600	0.700	5.00	0.800	0.800	2.20	2.40	2.30	0.900	1.80	2.06
Dy	15.1	14.9	10.3	11.0	3.60	15.4	14.1	5.80	6.30	3.60	3.50	3.40	4.00	34.1	5.80	5.10	13.7	15.5	13.3	5.60	2.40	4.43
Ho	2.70	2.70	2.10	2.20	0.700	3.10	2.90	1.10	1.20	0.800	0.700	0.600	0.800	7.00	1.20	1.00	2.80	3.10	2.80	1.20	0.300	0.810
Er	6.10	6.50	5.40	5.70	2.30	8.50	7.60	2.80	3.40	2.40	1.70	1.60	2.30	17.9	3.40	2.60	7.50	7.70	7.10	3.40	1.50	3.26
Yb	4.50	4.70	4.80	5.10	2.20	7.10	6.70	2.50	3.00	2.20	1.30	1.30	2.10	16.5	3.10	2.50	6.40	7.10	5.80	3.10	1.30	2.87
Lu	0.600	0.700	0.700	0.800	0.400	1.10	1.00	0.400	0.500	0.300	0.200	0.200	0.300	2.51	0.500	0.400	1.00	1.10	0.900	0.500	1.70	2.03
Hf	50.0	45.0	15.9	15.9	6.40	19.4	19.5	7.20	7.10	2.40	4.80	3.10	3.40	69.4	8.70	7.40	15.0	19.5	16.5	4.20	1.10	3.70
Th	26.8	25.9	28.8	24.9	10.4	36.9	31.0	11.0	21.7	5.20	9.30	0.800	29.0	82.1	9.40	12.8	27.4	38.0	28.4	6.90	4.20	7.50
U	3.80	5.10	2.50	1.90	4.70	4.00	4.50	4.70	3.60	6.10	6.30	6.60	6.90	2.80	2.90	6.40	4.30	2.50	3.40	5.10	5.90	2.10

Table 5. Selected 1470-1000 Ma palaeomagnetic poles from Baltica, Laurentia, Siberia and India.

	Rockname	Age (Ma)	Plat (°N)	Plong (°E)	A_{95} (°)	Reference
						Baltica
1[a]	Mean for Baltica	1480-1450	17	178.0	11.0	Lubnina et al. (2010)
2[b]	Mean for Baltica	~1265	4	158	4	Pesonen et al. (2003)
3	Salla Dyke VGP	1122±7	71	113	8	Salminen et al. (2009)
4[c]	Bamble Intrusions	1100-1040	3	217	15	in Meert and Torsvik (2003)
5	Laanila Dolerite	1045±50	-2	212	15	Mertanen et al. (1996)
						Laurentia
6[d]	Mean for Laurentia	1480-1450	-4.4	214.2	16.0	Pisarevsky and Bylund (2010)
7	MacKenzie dykes	1267+7/-3	4	190	5	Buchan and Halls (1990), LeCheminant and Heaman (1989)
8	Hviddal Dyke, Greenland	1184±5	33	215	10	Piper (1977); Upton et al. (2003)
9	Narssaq Gabbro, Greenland	1184±5	32	221	10	Piper (1977); Upton et al. (2003)
10	Giant Gabbro Dykes, Greenland	1163±2	42	226	9	Piper (1977); Buchan et al. (2001)
11	South Qoroq Intr., Greenland	1165-1160	42	216	13	Piper (1992)
12	Osler Volc.	1105±2	43	195	6	Halls (1974); Davis and Green (1997)
13[e]	Chengwatana Volc.	1095±2	31	186	8	Kean et al. (1997); Zartman et al. (1997)
14	Portage Lake Volc.	1095±3	27	178	5	Hnat et al. (2006); Davis and Paces (1990)
15	Cardenas Basalts	1091±5	32	185	8	Weil et al. (2003)
16	Lake Shore Traps	1087±2	22	181	5	Diehl and Haig (1994); Davis and Paces (1990)
17	Freda Sandstone	1050±30	2	179	4	Henry et al.(1977); Wingate et al. (2002)
18	Nonesuch Shale	1050±30	8	178	4	Henry et al.(1977); Wingate et al. (2002)
19	Chequamegon Sandst.	1050-990	-12	178	5	McCabe and Van der Voo (1983)

20	Jacobsville Sandstone	1050-990	-10	184	4	Roy and Robertson (1978)
21	Haliburton Intr.	1030-1000	-33	142	6	Warnock et al. (2000)
				Siberia		
22	Kyutingde, Sololi intrusions, Siberia	1473±24	33.6	253.1	10.4	Wingate et al. (2009)
23	Malgina Formation	1043±14	22	226	7	Gallet et al. (2000); Ovchinnikova et al. (2001)
24	Kumakha Formation	1040-1030	-14	201	7	Pavlov et al. (2000)
25	Milkon Formation	~1025	-6	196	4	Pavlov et al. (2000)
26	Nelkan Formation	1025-1015	-14	219	6	Pavlov et al. (2000)
27	Ignikan Formation	1015-1005	-16	201	4	Pavlov et al. (2000)
				India		
28	Lakhna Dykes, India	1465±3	36.6	132.8	14.0	This study
29	Harohalli alk. Dykes	1192±10	25	78	15	Pradhan et al. (2006)
30	Mahoba Dykes	1113±7	39	230	15	Pradhan et al. (2011)
31	Majhgawan Kim. VGP	1074±14	37	213	12	Gregory et al. (2006)
32	Anantapur Dykes	1027±13	9	213	11	Pradhan et al. (2010)

[a] Averaged from: Lubnina (2009), Bylund (1985), Salminen and Pesonen (2007), Lubnina et al. (2010).
[b] Averaged from: Neuvonen, 1965, 1966; Neuvonen and Grundström, 1969.
[c] Averaged from: Stearn and Piper, 1984.
[d] Averaged from: Meert and Stuckey (2002), Emslie et al. (1976), Irving et al. (1977).
[e] Without regional tilt correction.
VGP=Virtual Geomagnetic Pole

Table 6. Euler rotation parameters for Laurentia, Baltica and Siberia at 1460 – 1080 Ma (reconstructions in Figs. 11-15)

Craton	**Age** (Ma)	**Pole** Lat(°)	Lon(°)	**Angle** (°)
Laurentia to absolute framework	1460	-48.68	48.60	166.26
	1770	10.77	-17.29	-76.77
	1750	14.27	-14.48	-71.78
	1460	8.65	136.16	88.08
	1265	21.42	122.39	89.97
Baltica to Laurentia	1460-1270	44.99	7.45	44.93
	1120	-18.06	-126.33	-176.75
	1080	50.07	-83.97	-45.93
Greenland to Laurentia	1460-1080	67.50	241.52	-14.00
Siberia to Laurentia	1460-1080	66.60	139.30	134.80